frontiers | Frontiers in Marine Science

TYPE Original Research
PUBLISHED 25 March 2024
DOI 10.3389/fmars.2024.1378724

OPEN ACCESS

EDITED BY
Yang Yang,
Nanjing Normal University, China

REVIEWED BY
Bing Song,
Chinese Academy of Sciences (CAS), China
Xin Shan,
Ministry of Natural Resources, China
Qiang Zhang,
Chinese Academy of Sciences (CAS), China

*CORRESPONDENCE
Shihao Liu
shliu@sklec.ecnu.edu.cn
Shenliang Chen
slchen@sklec.ecnu.edu.cn

RECEIVED 30 January 2024
ACCEPTED 11 March 2024
PUBLISHED 25 March 2024

CITATION
Hu W, Liu S, Liu Y, Feng A, Feng W, Wang X and Chen S (2024) Pollen and spore records constrained by millennial prodelta evolution: a case study of the Huanghe (Yellow River) delta.
Front. Mar. Sci. 11:1378724.
doi: 10.3389/fmars.2024.1378724

Pollen and spore records constrained by millennial prodelta evolution: a case study of the Huanghe (Yellow River) delta

Weifen Hu[1], Shihao Liu[1*], Yan Liu[1], Aiping Feng[2,3], Wei Feng[1], Xiuhang Wang[1] and Shenliang Chen[1*]

[1]State Key Laboratory of Estuarine and Coastal Research, East China Normal University, Shanghai, China, [2]Fourth Institute of Oceanography, Ministry of Natural Resources, Beihai, China, [3]First Institute of Oceanography, Ministry of Natural Resources, Qingdao, China

Pollen and spore records in prodeltaic sediments hold significant potential for reconstructing paleoecologic and paleoclimatic evolution. However, uncertainties in these reconstructions arise from millennial-scale prodelta evolution, which dominates stratigraphic development and consequently influences sedimentary processes and/or pollen provenance. Here we explore the intricate relationship between pollen/spore records and prodelta stratigraphic evolution, using established seismic stratigraphy and ten sediment cores (five new, five from literature) within both the proximal and distal (mud belt) parts of the Huanghe (Yellow River) prodelta. In the proximal region, dominant lobate stratigraphic development, accompanied by shifts in river mouth and depocenter, leads to variations in pollen assemblages and contents within individual cores and differences in vertical pollen distribution across core sites. Transport distance appears to be a key factor, with arboreal pollens, particularly saccate ones (e.g., *Pinus*), positively correlating with the distance from the river mouth in their percentages within a single delta lobe, while non-arboreal and non-saccate arboreal pollens show higher percentages within shorter transport distances, despite longer distances leading to decreased total pollen concentrations. Likely due to the total pollen concentration after extended long-distance transport, this pattern is not observable in the distal mud belt. Subsurface stratigraphy in this mud belt reveals a complex pollen provenance characterized by *Artemisia-Ulmus-Chenopodiaceae-Pinus*, with non-arboreal pollens in dominance. Therein, non-arboreal pollens are not consistent with deposition from long-distance transport, and *Ulmus* pollens are uncommon in the western Bohai Sea. Interestingly, surface sediments in the mud belt display a different assemblage, characterized by *Pinus-Artemisia-Quercus*, consistent with the nearby Luanhe River prodelta, suggesting recent pollen supply from nearby sources, possibly due to the recent abandonment of the mud belt. Additionally, an energetic longshore transport/erosional regime reduces pollen content at the mud-belt margins and create pollen sinks (with the highest concentration) in the mud patch (accumulation area) within the erosion-dominated region adjacent to

the mud belt. Our findings confirm that stratigraphic evolution, alongside hydrodynamic conditions and pollen provenance, governs pollen assemblages in deltaic/prodeltaic sediments. They can provide insights for palynological and pollen-based paleoclimatic and paleoecologic studies in other deltas.

KEYWORDS

pollen transport, pollen preservation, prodelta, source-to-sink, Huanghe

1 Introduction

Pollen and spore are crucial environmental proxies widely utilized in the realm of paleoecology and paleoclimatology (Faegri and Iversen, 1989; Nakagawa et al., 2003; Di Rita et al., 2015). They have been extensively employed for paleoenvironmental and paleoclimatic reconstructions on river deltas, particularly on prodeltas (the subaqueous domain below fair-weather wave base, encompassing the mud belt and mud-dominated longshore dispersal system if present; Anthony et al., 2010; Korus and Fielding, 2015), which have long been recognized as significant sinks for terrestrial materials, holding great potential as sedimentary archives. Such reconstructions have been conducted worldwide on deltas, including those on the Pacific Ocean Coast (Yi et al., 2003, 2006; Li et al., 2006; Song et al., 2017; Hao et al., 2021; Ye et al., 2024), Atlantic Ocean Coast (Smith et al., 2020; Yao et al., 2020, 2022; Adojoh et al., 2023), Indian Ocean Coast (Hait and Behling, 2009; Mohapatra et al., 2019, 2021), and Mediterranean Coast (Pantaléon-Cano et al., 2003; Di Rita et al., 2015; Zhao et al., 2020).

However, within prodeltaic sediments, the pollen and spore records also bear to uncertainties to some extent, potentially influencing the aforementioned reconstructions. These uncertainties are predominantly attributed to the prodeltas' sensitivity to diverse sediment-transport and dispersal regimes, coupled with variations in riverine input fluxes and provenance during their development. Some scholars even propose that shifts in pollen assemblages in prodeltaic sediments are more likely linked to changes in depositional environments/processes rather than climate-related factors (Xu et al., 1996; DeBusk, 1997; Tian et al., 2008; Xu et al., 2016). This argument is partly supported by studies of pollen assemblages in modern seafloor sediments, which reveals influences from factors dominating sediment accumulation at such underwater environment, including oceanographic currents (e.g., tidal) and circulation (Heusser and Balsam, 1985), sediment transport (Sun et al., 1999; van der Kaars, 2001; Beaudouin et al., 2007), sediment density and grain size (Yang et al., 2019; Ouyang et al., 2021), and water depth and offshore distance (Hooghiemstra et al., 2006; Beaudouin et al., 2007; Luo et al., 2013; Yang et al., 2019).

Two aspects related to the evolution of prodelta can further complicate the aforementioned uncertainties and influence the pollen-based paleoenvironmental and paleoclimatic reconstruction: (1) the evolution of the prodelta may undergo complex cycles of deposition and erosion, as observed in deltas like the Huanghe (Yellow River) and Po River Deltas, characterized by frequent lobe switching (Correggiari et al., 2005; He et al., 2019), which can cause discontinuities in sedimentary archives; (2) the delta progradation is often accompanied by shoreline advancement, resulting in changes in the distance from the source, water depth, and marine dynamic processes over different intervals in one sediment core (Xue et al., 2018). Despite insights from modern prodelta sediments (seafloor samples; Chmura et al., 1999; Hooghiemstra et al., 2006; Yang et al., 2019; Ouyang et al., 2021), understanding how pollen and spore records within subsurface stratigraphy correlate with the sedimentary evolution of prodeltas, especially the influences from hydrodynamic conditions, transport regimes, and provenance during the evolution, remains less clear.

To address this issue, we focus on the Huanghe delta, particularly its prodelta in the western and northwestern Bohai Sea, in this study, which, renowned as one of the largest deltas on Earth, has been extensively studied for its sedimentary and stratigraphic evolution in recent years (He et al., 2019; Liu et al., 2019, 2020, 2022). Building on the well-established seismic stratigraphy (Liu et al., 2019; 2022), we utilized nine borehole cores and one gravity core (five newly acquired, five referenced from literature) (Table 1; Figure 1B) to establish seismic-to-core correlation and further examine the relationship between pollen and spore records and evolution of the prodelta stratigraphy. Our primary focus is to analyze variations in pollen and spore records within the same depositional interval in different prodelta locations, as well as to examine differences in pollen and spore assemblages between various depositional intervals, to identify the driving factors. We anticipate our findings will provide insights for pollen-based paleoenvironmental and paleoclimatic reconstructions in other deltaic regions.

2 The study area

2.1 Overview of Bohai Sea and its hydrodynamic conditions

The Bohai Sea covers ~77,000 km^2 and is characterized as an inland, shallow gulf (Liu et al., 2016a; He et al., 2019). The three

TABLE 1 Basic information of the cores examined in this study. Except for BH264, which is a gravity core, the others are borehole cores.

Core	Longitude (°E)	Latitude (°N)	Elevation (m)	Length (m)	Reference
BHB1	118.53	38.41	-15.8	20	This study
YRD1	119.49	38.00	-18	20	This study
H1	118.90	38.98	-20	30	This study
H3	119.56	39.31	-20	30	This study
H4	119.62	39.64	-15	30	This study
BH264	119.32	38.15	-20.1	2.95	Chen et al., 2012
H9601	118.48	37.68	5.5	22.5	Yi et al., 2003
H9602	118.91	37.80	4.9	28.3	Yi et al., 2003
H2	119.33	39.36	-18	30	Yu, 2019
L1	119.23	39.48	6.7	35	Yu, 2019

Elevations are referred to 1956 Yellow Sea height datum of China.

major bays within the Bohai Sea (Liaodong, Bohai, and Laizhou Bays) have a water depth of less than 20 m, except for the central Bohai Sea, where depths can reach up to 40 m (Qin et al., 1990). It is connected to the North Yellow Sea through a 104.3 km-wide passage, known as Bohai Strait, where the water depth can reach ~60 m (Figure 1A).

The Huanghe originates from the Tibetan Plateau, and flows across the Chinese Loess Plateau and the North China Plain. It is renowned for its substantial sediment load, and annually carries approximately 1.1×10^9 tons of sediment into the Bohai Sea over the past 2000 years (Milliman et al., 1987; Wang et al., 2007). The total sediment discharge from other rivers around the Bohai Sea is minimal, constituting only 3.6% of the Huanghe's sediment discharge (Xue et al., 2018).

Tidal patterns in the Bohai Sea are semidiurnal, with average and spring tidal ranges of 1.5-2 m and 3-4 m, respectively, in the western Bohai Sea (Xiong, 2012). Flood tidal currents can reach velocities of up to 5 knots (~2.5 m/s) around the north Bohai Strait

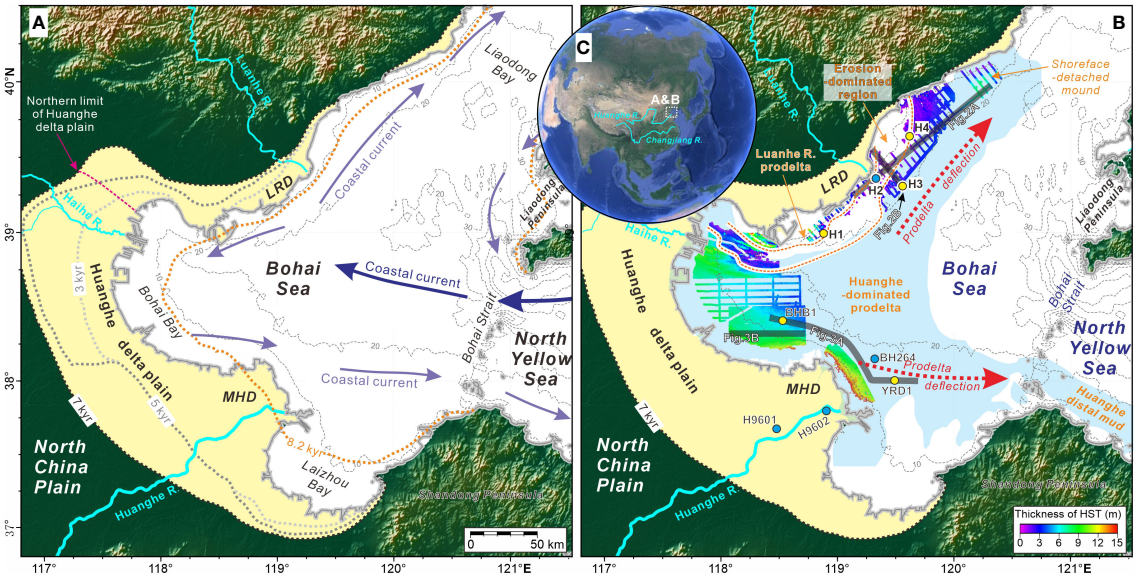

FIGURE 1
(A, B) Physiographic representation of the Bohai Sea, detailing bathymetry, present shoreline, and the delta plain formed since the mid-Holocene (yellow fill). In Panel **(A)**, historical shorelines (grey, black, and orange dashed lines with age labels) and the winter coastal current system (representative of long-term transport patterns) are superimposed (after Xue et al., 2018). Panel **(B)** illustrates subaqueous mud (blue fill) formed since the mid-Holocene highstand period, also known as the subaqueous highstand systems tract (HST), primarily composed of prodeltaic sediments (Liu et al., 2022). Isopachs of HST in the western and northwestern Bohai Sea, along with the positions of seismic profiles (bold black lines) and sediment cores from this study (yellow circles) and previously published data (blue circles) detailing in Figures 2–4, are indicated. Red dashed arrows indicate the directions of prodelta deflection in the Huanghe-dominated system. In the northwestern Bohai Sea, the Huanghe-dominated prodelta is separated from the Luanhe River prodelta by an elongated erosion-dominated region, delineated by heavy orange dashed lines. Modified after Liu et al. (2016a); Liu et al. (2019); Liu et al. (2022). Abbreviations: MHD=Modern Huanghe Delta; LRD=Luanhe River Delta; R.=river. **(C)** Overview of Bohai's location and full extension of the Huanghe and Changjiang Rivers.

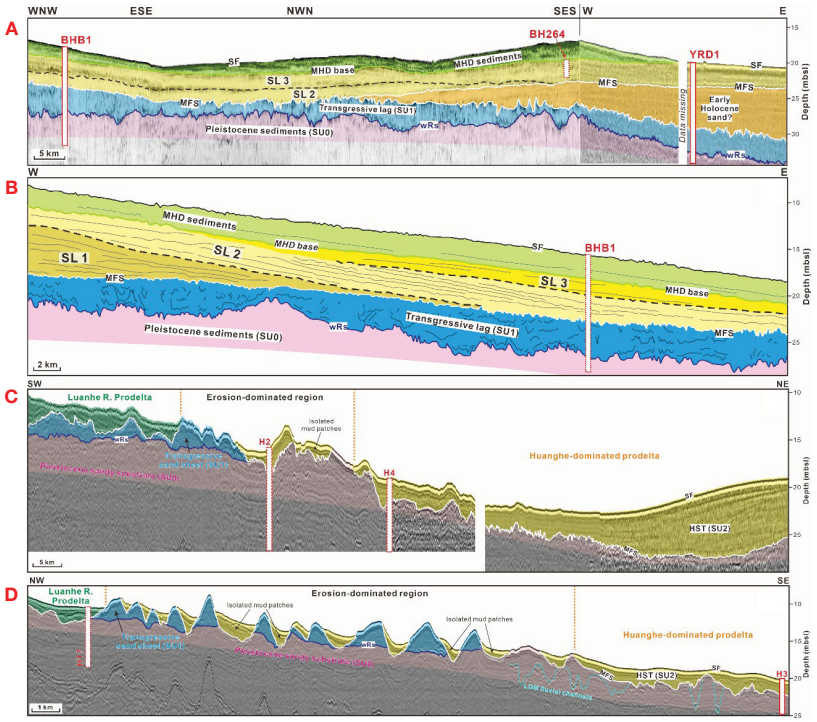

FIGURE 2
Interpreted seismic profiles covering approximately two-thirds of the offshore region around the MHD **(A)**, extending east-west north of MHD **(B)**, and along shore-parallel **(C)** and shore-normal **(D)** directions in the northwestern Bohai Sea, along with their correlation with sediment cores. The seismic interpretation in **(A, B)** follow Liu et al. (2019), with SUs 4-6 redefined as subaqueous lobes (SL) 1-3 in this study (the seismic profile in Panel **(A)** is a new addition from this study). **(C, D)** are modified from Liu et al. (2022), outlining boundaries of the Luanhe River prodelta, erosion-dominated area, and Huanghe-dominated prodelta with dashed orange lines. Solid-line columns represent sediment cores precisely aligned with seismic profiles, while dashed-line columns offer an approximate correspondence, emphasizing their relationship with seismic stratigraphy (especially for core H1 in Panel **D**). Refer to Figure 1B for profile and core locations, and see Supplementary Figure 2 and Table 1 for uninterpreted seismic profiles and core information, respectively. Abbreviations: LGM, Last Glacial Maximum; wRs, transgressive (wave) ravinement surface; MFS, Maximum flooding surface; SF, Seafloor.

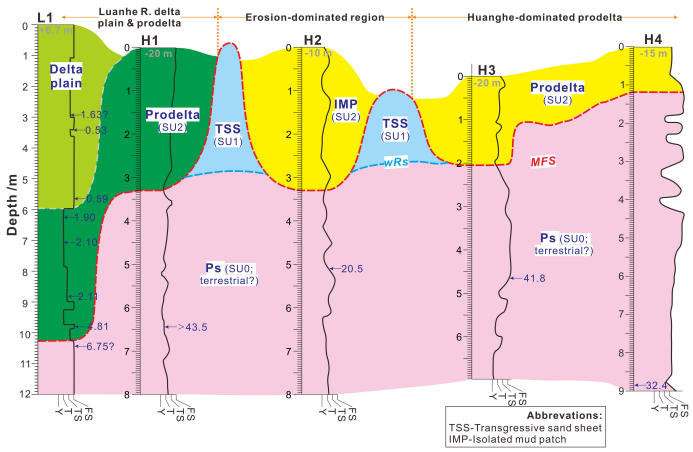

FIGURE 3
Stratigraphic transect of borehole cores L1 and H1-4 in the northwestern Bohai Sea. The stratigraphic pattern in the transect aligns with the seismic stratigraphic interpretation in Figures 2C, D and incorporates evidence from lithology and chronology from the cores. Basic information and radiocarbon ages along these cores are summarized in Tables 1–3, respectively. Note that there is a mismatch in the proportions of cores L1 and cores H1-H4. Please refer to legend in Figure 3 for additional details.

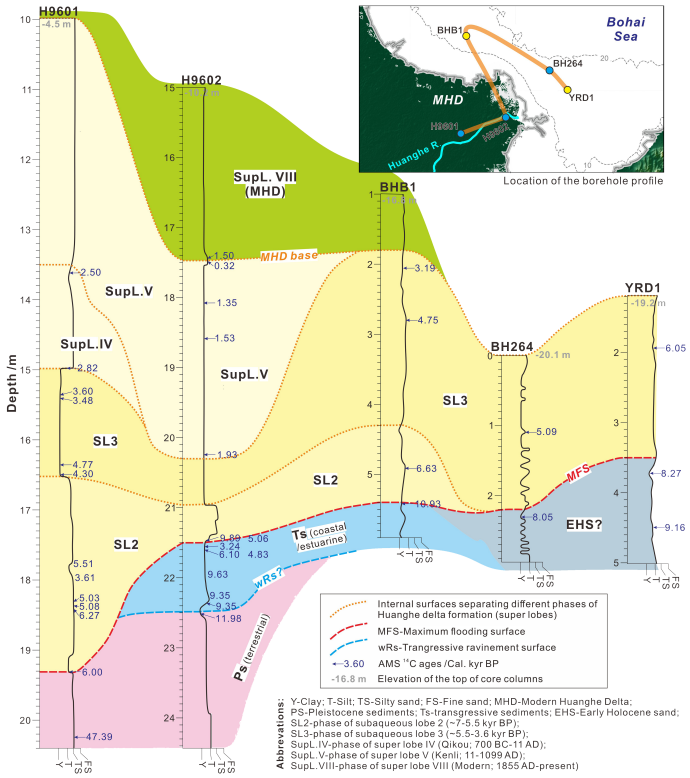

FIGURE 4
Stratigraphic transect of cores H9601, H9602, BHB1, BH264, and YRD1 in the vicinity of the MHD. The stratigraphic pattern in the transect corresponds to the seismic stratigraphic interpretation in Figures 2A, B and incorporates the documented stratigraphic divisions of the cores, along with evidence from lithology, chronology, and proxy indicators. The location of the transect is highlighted in the inset map with a bold orange line. Basic information and radiocarbon ages along these cores are summarized in Tables 1–3, respectively. The interpretation of delta formation phases aligns with the evolutionary history of super lobes in the delta plain (per He et al., 2019), detailed in Supplementary Figure 1.

(Liu et al., 2016a). The coastal current and oceanographic circulation within the Bohai Sea is predominantly influenced by high-salinity water from the Yellow Sea Warm Current, a branch of the Kuroshio Current. This circulation is counterclockwise in Liaodong Bay and clockwise in Bohai Bay (Liu et al., 2016a). The winter coastal current system, crucial for long-term sediment transport and prodelta evolution, is dominant because the Yellow Sea Warm Current is less intrusive in the summer; as a result, the circulation system predominantly transport river-borne sediments in winter, while storing them in summer (Su and Yuan, 2005; Xue et al., 2018). A bifurcation of the current occurs off the Luanhe River delta in the northwestern Bohai Sea (Figure 1A) (Su and Yuan, 2005; Liu et al., 2016a; 2016b).

2.2 Paleo-shoreline, delta evolution and subsurface stratigraphy

The Bohai Sea experienced transgression since the deglaciation period, and as an isolated gulf, seawater has entered Bohai Sea from the Bohai Strait since ~12 kyr BP. During the maximum flooding of the transgression ~7 kyr BP, the shoreline extended 50-90 km west of its present position (Xue, 1993; Xue et al., 2018). From the mid-Holocene onward, the shoreline advanced along the northern, western, and southern coasts of Bohai Bay, associated with the deltaic/alluvial progradation of the ancient Huanghe and other smaller river (e.g., Luanhe and Haihe Rivers) (Tian, 2010; Liu et al., 2019) (Figure 1A). These rivers, particularly the Huanghe, contribute the most sediment loads to the western and northwestern Bohai Sea (He et al., 2019).

The substantial sediment discharge originating from the Huanghe has played a crucial role in shaping the Huanghe delta both onshore (Xue, 1993; Saito et al., 2000; He et al., 2019) and offshore (Liu et al., 2009; Liu et al., 2016b, 2019) in the western Bohai Sea. The Huanghe River has experienced frequent avulsion and lobe-switching events (Cheng and Xue, 1997; Wang et al., 2007), leading to the formation of a deltaic plain comprised of distinct deltaic lobe (referred to as superlobes). Tranditionally, the delta plain was divided into 10 superlobes (Xue and Cheng, 1989; Xue, 2009), but a recent analysis of borehole cores along the western Bohai coast (He et al., 2019) has suggested a revised division into eight superlobes, accompanied by refined dating spans (Supplementary Figure 1A). Notably, except for the period from 1128 to 1855 AD when the Huanghe altered its course to the South Yellow Sea, forming a separate superlobe, all other superlobes are located along the western Bohai coast (Supplementary Figure 1A). North of the Huanghe delta plain, the northernmost regions of the western Bohai coast and the northwestern Bohai coast are

dominated by the Haihe and Luanhe River delta plains, respectively (Figure 1; Supplementary Figure 1A). Similar to the Huanghe delta plain, these areas have undergone evolution since the mid-Holocene, driven by the progradation of the two deltaic systems (Tian, 2010; Liu et al., 2019).

Offshore, there is a pervasive Huanghe-dominated mud region across the western, southern, and northwestern Bohai Sea (Figure 1B). The subaqueous delta clinoform of the Huanghe, as the subaqueous extension of the Huanghe delta plain, is situated predominantly in the western Bohai Sea with a thickness of up to 20 m (Figure 1B) (Liu et al., 2019). Dominated by eastward/southeastward and northeastward coastal currents, the Huanghe prodelta experiences deflection along these two directions, resulting in the formation of a unique dual-mud belt system (Figure 1B) (Liu et al., 2022). The eastward/southeastward deflected prodelta (mud belt) eventually reaches east of the Bohai Strait, entering the Yellow Sea and forming a mud wedge (up to ~40 m thick) offshore of the Shandong Peninsula (Yang and Liu, 2007). The northeastward deflected prodelta extends to the offshore regions of the Luanhe delta and even farther northeast, forming a depocenter (~10 m thick) near the furthest end of this mud belt (Figure 2C). This mud belt is separated from the adjacent Luanhe River prodelta (attached to the Luanhe River delta plain) by a shore-parallel erosion-dominated sandy region, which is ~10-20 km in width (Figure 1B) (Liu et al., 2022).

The seismic stratigraphy in the western and northwestern Bohai Sea has been extensively examined recently (Tian et al., 2017; Liu et al., 2019; 2020; 2022), providing a critical foundation for this research (Figure 2). Postglacial stratigraphy in these regions comprises three sets of stratigraphic units (Liu et al., 2020): (1) terrestrial sediments formed during Late Pleistocene when the study area was subaerially exposed and devoid of seawater influence, primarily representing the Lowstand Systems Tract; (2) transgressive lags formed during the transgression through winnowing processes, especially wave action and ocean currents, often exhibiting as sand sheets and corresponding to the Transgressive Systems Tract; and (3) a unit of prodelta sediments formed since the mid-Holocene due to the progradation of neighboring river deltas, representing the Highstand Systems Tract (HST). These units are bounded by a transgressive (wave) ravinement surface (wRs) and a Maximum Flooding Surface (MFS).

The focus of this study is on the HST, and its internal configuration reveals notable disparities between the western and northwestern Bohai Sea. In the former, the unit exhibits a lobate configuration, consisting of four subunits associated with the Huanghe-dominated prodelta (Liu et al., 2019; corresponding to seismic units 4-6 and 8 in that study) (Figure 2B). Therein, the most recent subunit represents the accumulation of the Modern Huanghe Delta (MHD) formed since 1855 CE. Its basal boundary truncates internal dipping reflections of the underlying subunits on their tops (Figure 2B), representing a regional erosional unconformity; this aligns with the shift of the Huanghe course to the South Yellow Sea between 1128 and 1855 CE, resulting in a lack of sediment supply and degradation of the prodelta in our study area (Liu et al., 2013; 2019). In the northwestern Bohai Sea, the HST is internally uniform, characterized by stratified reflections, with no lobate structure observed (Figures 2C, D). Due to energetic longshore transport regimes, transgressive sand sheets have transformed into a series of alongshore-arranged erosional ridges, a phenomenon particularly pronounced in the erosion-dominated region (Figures 2C, D). Consequently, HST sediments have been partitioned by this erosional region along the shore-normal direction, with (1) a wedge attached to the Luanhe River delta plain corresponding to the Luanhe River-dominated prodelta, (2) isolated mud patches filling the troughs among the ridges in the erosion-dominated area, and (3) the Huanghe-dominated prodelta, extending from coast to offshore (Figures 2C, D) (Liu et al., 2022).

2.3 Climate and vegetation

The Bohai Sea and its surrounding area are characterized by a warm and wet climate during summers and a cold and dry climate in winters, influenced by the East Asian Monsoon, with southerly and northerly winds prevailing in the summer and winter, respectively (Zang, 1996). The lowest temperatures (-1 to 4°C) typically occur in January, while the highest temperatures (24 to 27° C) are recorded in July and August. Precipitation is particularly concentrated in the summer, with an annual average of ~613.6 mm (IOCAS, 1985; Wang, 2013).

The vegetation surrounding the Bohai Sea (Supplementary Figure 1B) is predominantly characterized by deciduous broadleaved forests associated with warm temperate climates and shrub grasslands (Wang, 1993). Natural vegetation is predominantly observed in mountainous areas due to intensive agricultural and human activities on the plains (Meng and Wang, 1987). In the hills, deciduous broadleaved forests are dominated by *Quercus*, co-dominated with *Pinus*. Some deciduous broadleaved trees are present in the plain area, while others, e.g., *Betula*, *Tilia*, and *Carpinus*, are mainly found in the hills and lowlands. Coastal salt marshes are characterized by herb dominance, particularly *Chenopodiaceae* and *Artemisia* (Wang, 1993). Within the Huanghe delta plain, the vegetation is predominantly composed of herbs and shrubs, with trees dominated by *Pinus densiflora, Pinus tabuliformis*, and some other deciduous broadleaved forests. In the Luanhe delta plain, dominance is observed in *P. tabuliformis, Quercus liaotungensis*, and *Quercus dentate* (Supplementary Figure 1B).

In the Bohai Sea, the distribution of pollens and spores in seafloor sediments has been investigated by Yang et al. (2019), suggesting that Huanghe serves as the primary source. They also proposed that (1) pollen concentration is related to grain size, and (2) water depth is proportional to the percentages of *Pinus* pollen and *Pteridophyte* spores, while inversely related to other arboreal (excluding *Pinus*) and herbaceous pollen.

Previous palynological studies on sediment cores in this region primarily focused on paleoclimatic reconstruction (Yi et al., 2003; Chen et al., 2012; Lu et al., 2023), a scope does not align with the objective of this study. Nevertheless, these studies offer a valuable dataset for us to reevaluate the distribution of pollen and spore records in relation to the mid- and late-Holocene prodelta evolution.

3 Materials and methods

3.1 Seismic data

As mentioned earlier, the seismic stratigraphy in the western and northwestern Bohai Sea has been well characterized through recent investigations. To place our pollen records in the context of stratigraphic evolution via a seismic-to-core correlation, we employed three seismic profiles from these studies: one from the western Bohai Sea, extending east-west north of MHD (Liu et al., 2019), and two from the northwestern Bohai Sea along shore-parallel and shore-normal directions (Liu et al., 2022) (Figures 1B; 2B-D). The acquisition of these profiles utilized the Applied Acoustic Engineering CSP2200 subbottom system (United Kingdom). Additionally, we presented a new seismic profile covering approximately two-thirds of the offshore region around the MHD (Figures 1B; 2A). The eastern quarter of this profile employed the same subbottom system and firing parameters as the boomer profiles reported by Liu et al. (2022), while the western three-quarters utilized chirp data collected with an Edgetech 512i towfish featuring a 0.5-7.2 kHz, 30 ms pulse.

Seismic interpretation in the western and northwestern Bohai Sea followed Liu et al. (2019) and (2022), respectively. The interpretation of early Holocene sand and the overlying MFS at the location east of MHD was not addressed in Liu et al. (2019), as this sand body did not develop within their study area. These interpretations, instead, is based on the findings of Li et al. (2023) (detailed in section 4.1). Depth estimation used two-way travel time (TWTT) with an average acoustic velocity of 1650 m/s, following Liu et al. (2016a); Liu et al. (2019).

3.2 Sediment cores

Five new boreholes (BHB1, YRD1, H1, H3, and H4) were drilled in the western and northwestern Bohai Sea along with the seismic profiles (Figure 1B). The recovery rates for these cores exceed 90% (considering total length), except for the top 1 m of BHB1 and top 1.2 m of YRD1, which were unrecovered. Core positions were determined using DGPS. Given the primary focus on pollen records within prodeltaic sediments in this study, specific segments of these cores were selected for analysis: the top ~6 m of core BHB1 and the top 5 m of cores YRD1, H1, H3-H4. The selection of these segments was based on their correlation with the seismic stratigraphy. In the laboratory, these segments were longitudinally split, described, photographed, and subsampled for subsequent analysis. Additionally, five sediment cores (H9601, H9602, BH264, L1, H2) were sourced from existing literature, selected based on established chronological constraints and palynological data availability.

Cores BHB1, YRD1, H9601, H9602, and BH264 are situated in the western Bohai Sea, both onshore and offshore of the Huanghe delta plain. The remaining five boreholes (L1 and H1–4) are located in the northwestern Bohai Sea, both onshore and offshore of the Luanhe River Delta (Figure 1B). Basic information for these cores is summarized in Table 1.

3.3 Sediment sample measurement and analysis

Ten samples (including bulk sediments, peat, plant and benthic foraminifera) from the newly acquired cores were selected for ^{14}C dating at Beta Analytic Inc. (Miami, United States) and Pilot National Laboratory for Marine science and Technology (Qingdao, China) using accelerator mass spectrometry (AMS). Past research in and around the Bohai Sea has suggested that conventional ages of marine samples should be calibrated using the Marine curve when their $\delta^{13}C$ values exceed -10‰, while the IntCal curve is more appropriate for values typically around -25‰ (e.g., He et al., 2018; Liu et al., 2023). Given this, our bulk sediment, peat, and plant samples, characterized by $\delta^{13}C$ values nearing −25‰, were calibrated using the latest IntCal 20 curve, while shell and benthic foraminifera samples were calibrated using the most recent Marine 20 model (Reimer et al., 2020) with the ΔR=-334 ± 50. All calibrations were conducted using Calib Rev. 8.2 software with a two standard deviation (2σ) of uncertainty (Stuiver et al., 2022).

Thirty-nine AMS ^{14}C ages have been documented along with the other five cores (from literature sources), but they were not calibrated with the same standards (i.e., the Marine20 and IntCal20 models were not used). In this regard, a recalibration was conducted using these latest models. The dating (and calibration/recalibration) results newly reported in this study and those from earlier research are summarized in Tables 2, 3, respectively.

A total of 178 samples were collected at 5-10 cm intervals (for cores BHB1 and YRD1) and 15-20 cm (for cores H1, H3 and H4) intervals for grain size analysis. The grain size data were determined using a Malvern Mastersizer-2000 laser particle size analyzer (United Kingdom) after pretreating the samples with 10% H_2O_2 and 0.1 N HCl to remove organic matter and biogenic carbonate. The grain size parameters (e.g., mean diameter) were calculated following the procedure of Folk and Ward (1957). The classification of sediment types was determined using the classification scheme established by Shepard (1954).

Fifty-two samples were taken at 5-30 cm (for cores YRD1 and BHB1) or 50-100 cm (for cores H1, H3 and H4) intervals for pollen and spore analysis. Each sample, weighing 5.0 ± 0.3 g (cores YRD1 and BHB1) or 10.0 ± 0.3 g (cores H1, H3 and H4) in dry weight, were processed following the presentative palynological treatment procedures (Moore et al., 1991). This involved the use of 10% HCl to dissolve calcareous minerals, 10% KOH treatment for the removal of organic matter, and 45% HF to eliminate siliceous materials. The residues were sieved over a 7-mm mesh screen in an ultrasonic water bath to remove tiny impurities and facilitate pollen identification. To facilitate identification, exotic *Lycopodium* marker spores (10,315 ± 281 grains/tablet) were added before the initial sample treatment. The prepared specimens were subsequently mounted in glycerin jelly for examination and identification.

Pollen identification and counting were conducted using a Nikon Eclipse Ni stereomicroscope at 400× or 1000× magnification. Palynomorphs were identified in accordance with

TABLE 2 Accelerator mass spectrometry (AMS) ^{14}C ages obtained from borehole cores newly reported in this study.

Core	Depth(m)	Materials	$\delta^{13}C$/‰	Conventional age (yr BP)	Calendar ages (cal yr BP)		Lab. Code
					Medium	Range (2σ)	
BHB1	2.07	Benthic foraminifera		3155 ± 25	3188	2993-3383	QNLMA 220362
	2.84	Bulk sediments	-25.7	4220 ± 30	4749	4644-4853	Beta-584378
	4.92	Bulk sediments	-22.8	5820 ± 30	6634	6536-6732	Beta-640519
	5.41	Peat	-21.3	9580 ± 30	10927	10749-11104	Beta-652513
YRD1	1.90	Bulk sediments	-22.5	5250 ± 30	6052	5928-6176	Beta-640521
	3.69	Bulk sediments	-24.1	7450 ± 30	8266	8187-8345	Beta-640522
	4.57	Bulk sediments	-23.2	8210 ± 30	9155	9026-9283	Beta-580364
H1	6.45	Bulk sediments	-25.2	> 43500 BP			Beta-408089
H3	4.65	Plant	-28.5	37060 ± 330	41770	41344-42195	Beta-408101
H4	8.84	Bulk sediments	-24.5	28260 ± 130	32405	31854-32956	Beta-408107

TABLE 3 AMS ^{14}C ages from previously published cores.

Core	Depth (m)	Materials	$\delta^{13}C$ (‰)	Conventional age (yr BP)	Calendar ages (cal yr BP)		Code	Reference
					Intercept	Range (2σ)		
H9601	13.6	*Scapharca subcrenata (Lischke)*	-0.2	2560 ± 50	2499	2287-2711	Beta-105713	Yi et al., 2003
	14.97	*Tellinella* sp.	-10.5	2830 ± 40	2816	2613-3019	Beta-108225	Yi et al., 2003
	15.37	*Dosinella penicillata (Reeve)*	-3.0	3480 ± 50	3599	3379-3820	Beta-105720	Yi et al., 2003
	15.4	*Glassaulax vesicalis (Philippi)*	-3.2	3390 ± 50	3481	3260-3702	Beta-105721	Yi et al., 2003
	16.35	*Scapharca subcrenata (Lischke)*	-0.4	4390 ± 50	4766	4525-5008	Beta-105722	Yi et al., 2003
	16.52	*Scapharca subcrenata (Lischke)*	-0.4	4020 ± 50	4298	4057-4539	Beta-105714	Yi et al., 2003
	17.8	Shell fragments	-1.6	5010 ± 60	5514	5301-5728	Beta-105723	Yi et al., 2003
	17.95	*Scapharca subcrenata (Lischke)*	-1.2	3490 ± 50	3608	3387-3829	Beta-105715	Yi et al., 2003
	18.33	*Crassostrea sp*	-1.0	4570 ± 60	5033	4793-5274	Beta-108226	Yi et al., 2003
	18.37	*Zeuxis squinjoreusis (A. Adams)*	-2.1	4640 ± 50	5079	4854-5304	Beta-105716	Yi et al., 2003
	18.4	*Scapharca subcrenata (Lischke)*	-0.5	5710 ± 50	6268	6056-6480	Beta-105717	Yi et al., 2003
	19.35	*Scapharca broughtonii (Schrenck)*	-0.3	5460 ± 50	6002	5786-6219	Beta-108224	Yi et al., 2003
	22.60	Shell fragments	-1.2	47390 ± 1500			Beta-105718	Yi et al., 2003
H9602	17.48	*Naticidae genus et speces indet.*	-6.1	1750 ± 40	1495	1309-1682	Beta-108227	Yi et al., 2003

(Continued)

10.3389/fmars.2024.1378724

TABLE 3 Continued

Core	Depth (m)	Materials	$\delta^{13}C$ (‰)	Conventional age (yr BP)	Calendar ages (cal yr BP)		Code	Reference
					Intercept	Range (2σ)		
	17.5	*Monia* sp., *Microcirce dilecta (Gould)*	1.2	550 ± 50	324	144-505	Beta-105724	Yi et al., 2003
	18.06	*Phacosoma* sp.	-0.8	1620 ± 40	1352	1176-1529	Beta-108228	Yi et al., 2003
	18.60	Shell fragments	0.0	1790 ± 70	1530	1304-1757	Beta-108229	Yi et al., 2003
	20.25	*Echinoid fragments Tellinella*	-1.9	2130 ± 40	1933	1723-2144	Beta-108230	Yi et al., 2003
	21.48	*Chloromytilus viridis (Linnaeus)*	-10.3	8950 ± 50	9890	9627-10153	Beta-105725	Yi et al., 2003
	21.48	*Ringicula (Ringiculina) doliaris (Gould)*	-1.8	4610 ± 50	5059	4836-5283	Beta-105726	Yi et al., 2003
	21.53	*Laevidentalium* sp.	0.5	3200 ± 50	3239	3020-3458	Beta-105727	Yi et al., 2003
	21.57	*Corbicula (Corbiculina) leana (Prime)*	-1.8	5550 ± 50	6095	5902-6288	Beta-105728	Yi et al., 2003
	21.57	*Ringicula (Ringiculina) doliaris (Gould)*	-1.3	4440 ± 40	4828	4589-5068	Beta-105729	Yi et al., 2003
	21.98	Shell fragments	-7.8	8720 ± 60	9626	9382-9871	Beta-108231	Yi et al., 2003
	22.25	*Corbicula (Corbiculina) leana (Prime)*	-9.6	8540 ± 40	9350	9165-9535	Beta-105730	Yi et al., 2003
	22.37	*Littoraria coccinea (Gmelin)*	-8.7	8550 ± 60	9348	9129-9568	Beta-108232	Yi et al., 2003
	22.5	*Littoraria coccinea (Gmelin)*	-9.8	9160 ± 60	10168	9900-10436	Beta-108233	Yi et al., 2003
BH264	1.11	Benthic foraminifera	-2	4650 ± 35	5089	4874-5303		Chen et al., 2012
	2.29	Benthic foraminifera	-2	7430 ± 50	8053	7852-8254		Chen et al., 2012
H2	5.1	Sediment	-23.6	17090 ± 51	20475	20499-20814	Beta-408093	Yu, 2019
L1	2.95	Shell	2.8	1880 ± 30	1632*	1437-1826		Yu, 2019
	3.42	Plant	-27.1	500 ± 30	526	501-550	Beta-418975	Yu, 2019
	5.75	Plant	-26.3	575 ± 30	587	529-644		Yu, 2019
	6.2	Shell	1.8	2100 ± 30	1903	1706-2100		Yu, 2019
	7.1	Shell	-1.9	2250 ± 30	2098	1896-2299	Beta-418976	Yu, 2019
	8.98	Shell	-1.5	2260 ± 30	2109	1909-2306		Yu, 2019
	9.8	Shell	0.9	4420 ± 30	4808	4586-5029		Yu, 2019
	10.44	Shell	1.1	6150 ± 30	6753*	6549-6957		Yu, 2019
	14.5	Wood	-25.7	41250 ± 340	44022	43351-44692	Beta-418978	Yu, 2019

All these ages were previously reported, and their references are provided. In this study, we recalibrated the calendar ages using the latest models (Marine20 and Intcal20). *indicates ages that do not align well with the stratigraphic pattern in Figure 3.

the Quaternary Pollen Atlas (Wang et al., 1995; Tang et al., 2020). For each sample, a minimum of 200 pollen grains (excluding spores) were counted. A pollen diagram was created using TILIA 2.0.29 (Grimm, 1991 and the subsequent updated version). The pollen and spore percentages, indicating relative concentrations, were calculated based on the terrigenous pollens and spores.

4 Results

4.1 Stratigraphic framework

All ten sediment cores examined in this study have been integrated into the pre-existing seismic stratigraphic framework (section 2.2), utilizing seismic-to-core correlation (Figures 2A-D) and incorporating AMS ^{14}C dating results (Tables 2, 3). Stratigraphic transects of the core columns, integrated with the seismic stratigraphic framework, from the western and northwestern Bohai Sea are depicted in Figures 3, 4, respectively. The variations in mean grain size for the five newly acquired cores are illustrated in Figures 5–9.

4.1.1 Stratigraphy in western Bohai Sea

To simplify the description of seismic stratigraphy, we redefined the lobate subunits within the Huanghe prodelta, which corresponds to the HST, as subaqueous lobes (SLs), with SLs 1-3 and the lobe associated with MHD corresponding to seismic units 4-6, and 8 in Liu et al. (2019), respectively (Figures 2A, B). In core BHB1, HST sediments locate in the top 5.4 m and cover SL2, SL3, and the MHD lobe, from bottom to top. The sediments below 5.4 m is dominated by transgressive coastal/estuarine muds, with a peat layer observable inside dating to 10.93 cal. kyr BP (Figure 4). In core YRD1, HST sediments correspond to SL3 in the top 3.5 m; a similar corresponding relation is also identifiable in core BH264. Below the HST sediments in both cores YRD1 and BH264 lies a sand unit formed during the early Holocene (~8-9.2 kyr) (Figure 4), extending thicker seaward but thinning and displaying apparent truncation landward (Figure 2A). This sand body appears to align with the early Holocene depocenter in the southern Bohai Sea documented by Li et al. (2023), corresponding to the Transgressive Systems Tract.

Based on the ages of SLs 2 and 3 (Figure 4), despite some deviation, the two lobes likely correspond to superlobes I (~7-5.5 kyr BP) and II (~5.5-3.6 kyr BP) in the Huanghe delta plain (Supplementary Figure 1A). As for onshore boreholes H9601 and H9602, although seismic-to-core correlation is not achievable, we establish correlation between sediment intervals in these cores and delta lobes based on abundant previously reported chronological and sedimentological (especially lithological changes) data (Figure 4). SLs 2-3 have been identified within both cores, situated at relatively deeper portions of the cores (~15 to 19.3 m in core H9601 and ~20.3-21.5 in core H9602). Several younger lobes formed ~3-1 kyr BP overlie these two lobes, where over half sediments originate from the MHD (Figure 4).

4.1.2 Stratigraphy in northwestern Bohai Sea

The four offshore boreholes (H1-H4) do not penetrate on the ridge-shaped transgressive sand sheets (Figures 2C, D). Instead, ~2-3 m thick HST sediments (SU2) at their uppermost sections (lacking dating for confirming the formation age) overlie directly late Pleistocene terrestrial sand bodies, which dated older than ~20 kyr BP, reaching to 41.5 kyr BP (Figure 3). HST sediments in the four cores are situated in different zones that have been introduced in section 2.2: the unit in core H1 and those in cores H3 and H4 are positioned in the Luanhe River prodelta and Huanghe-dominated prodelta, respectively; the unit in core H2 is within the erosion-dominated area but corresponds to isolated mud patch, an area of accumulation/erosional remnants (Figure 3). Notably, HST sediments in cores H1 and H4 represent the marginal deposition of prodeltas because the two cores are located at the boundary

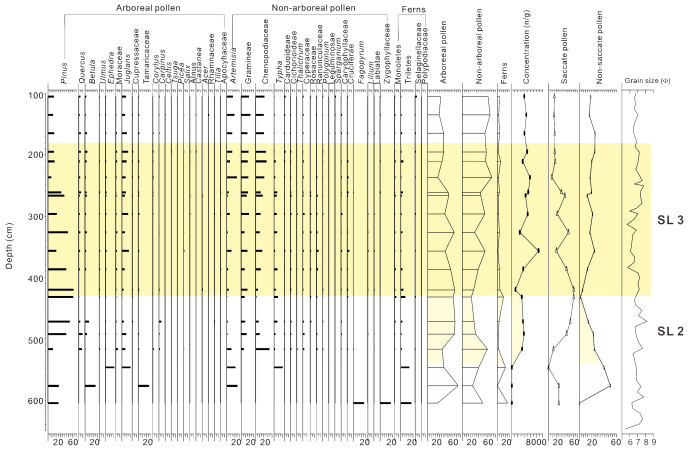

FIGURE 5
Downcore distribution of palynomorphs (percentage and concentration) and mean grain size recorded from borehole BHB1. Supplementary Figure 3 depicts the downcore distribution of grain size component of this core, as well as cores YRD1, L1, and H1-H4.

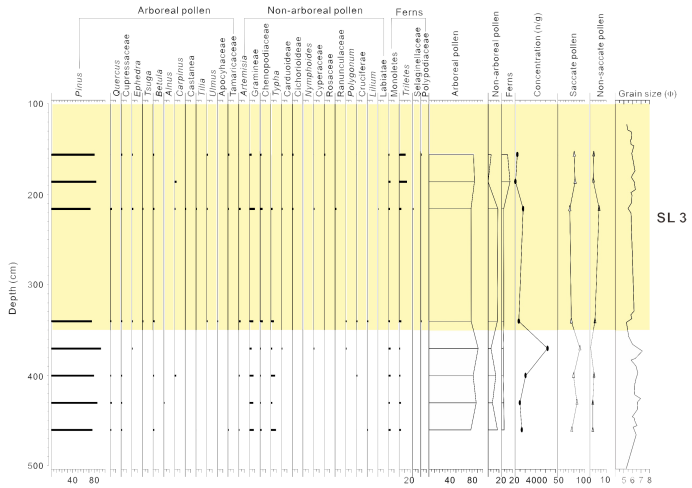

FIGURE 6
Downcore distribution of palynomorphs (percentage and concentration) and mean grain size recorded from borehole YRD1.

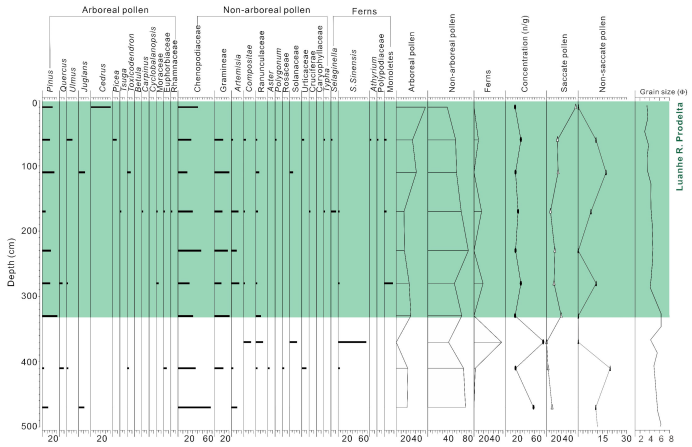

FIGURE 7
Downcore distribution of palynomorphs (percentage and concentration) and mean grain size recorded from borehole H1.

between the prodeltas and the erosion-dominated area (Figure 1B). The onshore borehole L1 is characterized by HST sediments exceeding 10 m in thickness, which encompasses a unit of Luanhe River prodelta in the lower part (~6-10.2 m) and a unit of Luanhe River delta plain in the upper part (0-6 m) (Figure 3).

4.2 Pollen records

In the five newly acquired boreholes, over 80 sporopollen types were identified, predominantly originating from deciduous trees and herbs (Figures 5–9). Therein, the arboreal pollens (AP) were dominated by gymnosperms, particularly *Pinus* and *Picea*, while angiosperm pollens included mainly deciduous *Quercus*, *Betula*, *Ulmus*, *Ephedra*, *Morus*, and *Carpinus*. Non-arboreal pollen (NAP) grains were mainly composed of *Artemisia*, Gramineae, Chenopodiaceae, *Typha*, and Cyperaceae. Fern spores included *Selaginella*, Triletes, and unidentified Monoletes. Pollen concentrations ranged from 1 to 8723 grains/g, with varying percentages and concentrations of AP and NAP. *Pinus* was notably abundant in several sections (Figures 5-9).

4.2.1 Pollen assemblage in western Bohai Sea

The two cores in the western Bohai Sea (BHB1 and YRD1) reveal diverse palynomorph assemblages; a total of 58 palynoflora, including 47 pollen, 5 spores, and 6 algae, were identified (Figures 5, 6). The average concentration and percentage of AP are greater than those of NAP. For the AP pollen, the gymnosperm pollen is dominated by *Pinus*, while the angiosperm pollen predominantly consists of deciduous *Quercus, Betula, Ephedra*, and Moraceae. NAP grains were primarily composed of *Artemisia*, Gramineae, Chenopodiaceae, and *Typha*. Fern spores and algae are dominated by Triletes, and Spiniferitaceae and Zygnemataceae, respectively.

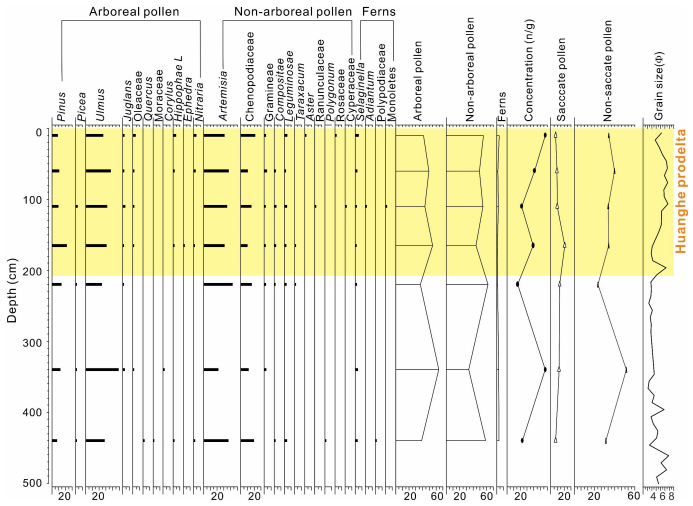

FIGURE 8
Downcore distribution of palynomorphs (percentage and concentration) and mean grain size recorded from borehole H3.

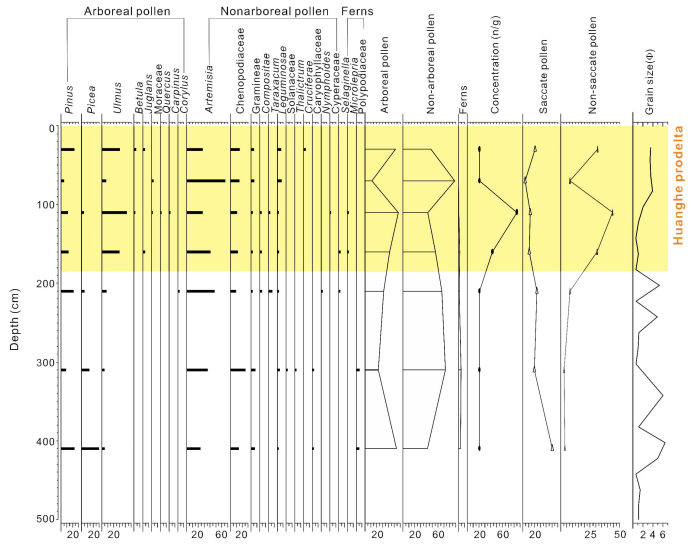

FIGURE 9
Downcore distribution of palynomorphs (percentage and concentration) and mean grain size recorded from borehole H4. Additional distributions of palynomorphs in cores L1 and H2 are presented in Supplementary Figures 4, 5, respectively, as they were solely published in a Chinese dissertation, potentially limiting accessibility.

4.2.1.1 Pollen assemblage in core BHB1

As mentioned earlier, BHB1 predominantly encompasses two lobes, i.e., SLs 2 and 3 (Figure 4). Pollen records associated with SL2 were dominated by AP, primarily consisting of *Pinus* (~52%), and NAP, mainly comprising Chenopodiaceae (~13%). The average pollen concentration is ~3500 grains/g. Notably, Gramineae (~8.8%), *Typha* (~4.9%), *Quercus* (~4.4%), and *Artemisia* (~3.3%) exhibited relatively high concentration (Figure 5). The frequency and concentration of AP remained high throughout this segment, but gradually increase toward the upper boundary of the segment, while that of NAP decreased upwards (Figure 5). Saccate pollen (SP) was abundant and exhibited a significant trend of upward increasing, which is contrasting with the distribution of non-saccate arboreal pollen (NSP). Fern spores were scarce, but their frequency and concentration increased upwards in this zone (Figure 5).

In SL3, the average pollen concentration exceeded 4500 grains/g, which surpasses SL2 (Figure 5). The percentage and concentration of NAP were slightly higher than those of AP. Prominent AP elements (i.e., that with high percentage) included *Pinus* (~30%), and prominent NAP elements comprised Chenopodiaceae (~15%). Other accessory elements in this segment featured pollen grains of Gramineae (~13.8%), *Artemisia* (~7.3%), *Typha* (~4.2%), *Quercus* (~2.2%), Betulaceae (~1.6%), and ferns (~1.3%). The NSP, in contrast to that within SL2, exhibits a trend of decrease upward (Figure 5).

4.2.1.2 Pollen assemblage in core YRD1

SL3 in core YRD1, the exclusive lobe covered in the core (Figure 4), shows a relatively lower average pollen concentration (~720 grains/g) compared to core BHB1 (Figure 5). The AP were much greater than NAP in frequency and concentration. Therein, AP constitutes ~82% of the total concentration, primarily comprising *Pinus* (~77%) and Betulaceae (~0.7%), while NAP account for ~10.3%, dominated by Gramineae (~4.3%), Chenopodiaceae (~2%), and *Artemisia* (~1%). The prevalent fern spore taxa include Triletes (~7.2%) and Monoletes (~1.2%). The SP (~83%) was significantly greater than NSP (~12%) in terms of the percentage, and shows a slight trend of increase upward (Figure 6).

4.2.2 Pollen assemblage in northwestern Bohai Sea

In the northwestern Bohai Sea, a total of 41 palynoflora, comprising 33 pollens and 8 spores, were identified in cores H1, H3, and H4. These cores exhibit low pollen concentrations ranging from 21 to 85 grains/g, with NAP percentages generally surpassing those of AP. Specific pollen records reveal that gymnosperm pollen is predominantly *Pinus* and *Picea*, angiosperm pollen is characterized by deciduous *Ulmus* and *Juglans*, and NAP grains consisted mainly of *Artemisia*, Chenopodiaceae, and Gramineae. Fern spores and algae were rare (Figures 7-9).

4.2.2.1 Pollen assemblage in core H1

The prodeltaic sediments (SU2; HST) in core H1 exhibit poorly preservation state of pollen characterized by low concentrations ranging from 21 to 33 grains/g (Figure 7). Within this segment, NAP prevails as the dominant pollen element, constituting ~61.8% of the total concentration, and it is primarily composed of Chenopodiaceae (~30.3%), Gramineae (~18.8%), and *Artemisia* (~5.8%). AP is also present but with a low concentration, mainly attributed to *Pinus* (~18%) and *Ulmus* (~1.9%). The percentage frequency of NAP and NSP exhibits a gentle decrease upwards. Conversely, the percentages of AP and SP show slight fluctuations (Figure 7).

4.2.2.2 Pollen assemblage in core H3

The HST sediments within this core exhibit a low pollen concentration ranging between 22 and 57 grains/g. The AP and NAP contribute almost equally to the total pollen content within this section. Specifically, *Artemisia* and Chenopodiaceae dominate the AP component, constituting ~32.2% and 13.3%, respectively, while *Ulmus* and *Pinus* are the predominant contributors to NAP, accounting for ~30.3% and ~11.3%, respectively (Figure 8). The percentage and frequency of NAP and NSP show a trend of upward increase, while that of AP and SP show an opposite trend of decrease slightly upward (Figure 8).

4.2.2.3 Pollen assemblage in core H4

The pollen assemblage from HST sediments in core H4 displays consistently low concentrations, ranging from 21 to 85 grains/g (Figure 9). It shows a pattern aligns with the observations from core H3, where both NAP and AP were equally abundant and t dominant elements within these two components are consistent with those in core H3. Specifically, NAP is characterized by *Artemisia* and Chenopodiaceae, contributing ~38.8% and ~12%, respectively, while AP is dominated by *Ulmus* and *Pinus*, comprising ~26% and ~11.6%, respectively. A notable feature in core H4 is the significant predominance of SP, accounting for approximately ~85%, compared to SP, which represents only ~15%. The percentage and frequency trends of both NAP and AP, as well as NSP and SP, exhibit fluctuations. Additionally, the presence of fern spores is rare, and algae are entirely absent within this core (Figure 9).

5 Discussion

Examining core transects in both proximity and distal to the sediment source (i.e., the contemporaneous Huanghe mouth) (Figure 1B), allow us to investigate how pollen and spore records respond to a range of environmental factors associated with prodelta evolution. In the western Bohai Sea (proximal location), the stratigraphic evolution is primarily influenced by the spatial-temporal dynamics of Huanghe's delta lobes (He et al., 2019; Liu et al., 2019). The cores (Figure 4) offer insights into how pollen records respond to the lobe-switching-dominated evolution and sediment dispersal. In the northwestern Bohai Sea (distal position), the stratigraphy is characterized by a longshore erosion-dominated area, leading to the separation of the Huanghe-dominated mud belt from the Luanhe River prodelta (Figure 3). Situated in different zones, these cores provide understanding of pollen records in response to the distal accumulation associated with complex provenance and hydrodynamic conditions.

In this section, we organize our discuss around individual influence of these factors. We acknowledge that some pollen records may be affected by the interaction of two or more factors, which will be addressed in the relevant text. To facilitate this analysis, we present the concentration and percentage of representative pollen elements from each core along with stratigraphic transects (Figures 10, 11 and Supplementary Figures 6, 7). The selection of pollen elements is based on their significant percentages and distinct distribution patterns identified in earlier studies on pollen assemblages within the surficial sediments (Yang et al., 2019), as well as in sediment cores analyzed in this study.

5.1 Pollen records in relation to sediment dispersal distance

In the proximal core transect, core BHB1 shows the highest percentages of SP and AP for SL2, while core YRD1 exhibits the highest percentages for SL3 (Figure 10). Considering the alignment of SLs 2 and 3 with superlobes I and II on the Huanghe delta plain, along with the locations of these superlobes and contemporaneous

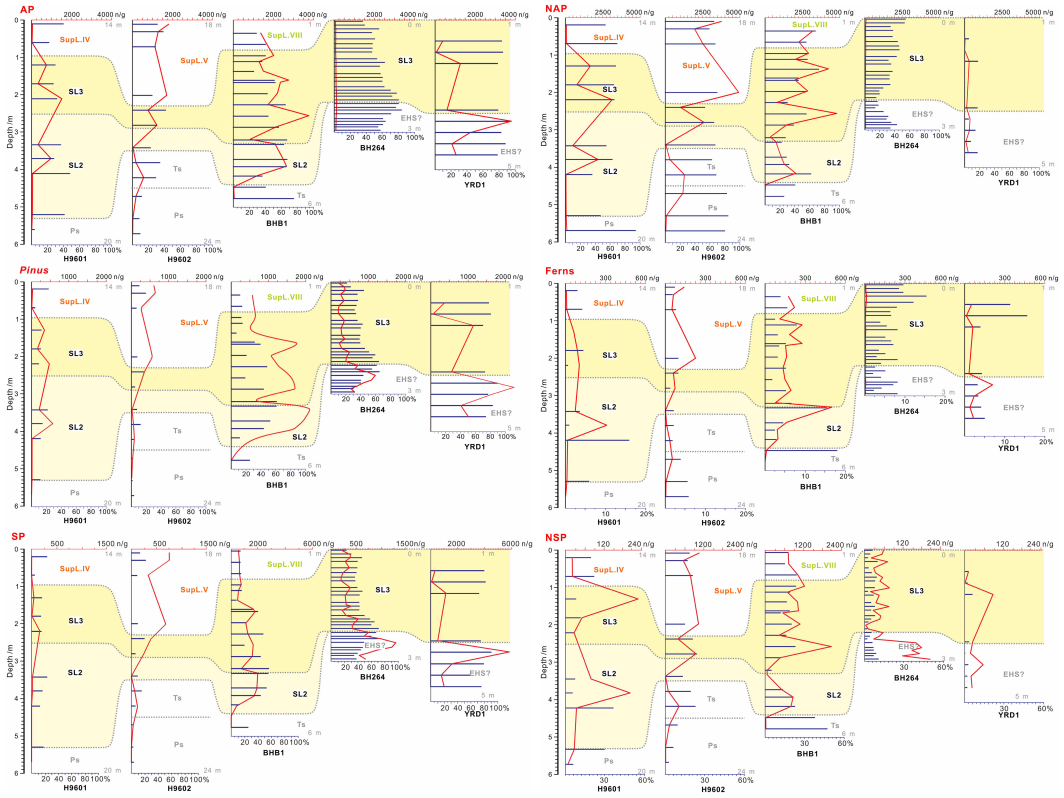

FIGURE 10
Concentration (grains/g; red curves) and percentage (navy bars) of representative pollen assemblages along the subsurface core transect of the Huanghe delta plain and subaqueous delta; see Figure 4 for the stratigraphic interpretation of the transect. The gray numbers on the right side of the diagrams indicate the depth of the section presented from each core. In this figure and Figure 11, only a subset of representative pollen elements is shown for the two core transects; additional elements along the two transects are detailed in Supplementary Figures 6, 7. AP, arboreal pollen; NAP, non-arboreal pollen.

paleo-shorelines, core YRD1 is the farthest core site from the contemporaneous Huanghe mouth along the direction of the offshore sediment dispersal regime during the evolution of SL3/superlobe II, and core BHB1, although not the farthest, is situated far away from the Huanghe mouth and within the upcurrent location of the sediment dispersal regime during the formation of SL2/superlobe I (Figure 1A; Supplementary Figure 1A). From a source-to-sink perspective, the upcurrent location can also be considered a considerably far distance for sediment transport, as it is not the typical destination for sediment deposition. In this context, our observation suggests that SP and AP can disperse to more distant locations in the proximal region, aligning with previous studies indicating that pollen with air sacs can travel greater distances compared to NSP (Wodehouse, 1935; Schwendemann et al., 2007; Leslie, 2010). The consistent dispersal pattern between SP and AP is likely due to a significant portion of AP consisting of airborne pollen species (Nilsson et al., 1977; Rahman et al., 2020). These findings also extend to individual pollen species; *Pinus*, a representative species of SP due to its lightweight nature allowing it to float in both water and air for an extended period with two air sacs (Schwendemann et al., 2007), shows a consistent increase in percentage within both SLs 2 and 3 as the transport distance increases (Figure 10).

Contrastingly, core BHB1 exhibits the lowest percentages for NSP and NAP in SL2, while core YRD1 shows the lowest percentages for SL3 (Figure 10). This suggests that the dispersal of NSP and NAP differs from that of SP and AP and is not dominant in long-distance transport. Despite NAP grains being generally smaller than AP and presumably dominated by water transport over longer distances, both NAP and *Artemisia* (a representative NAP species) show decreasing percentages with dispersal distance in SL2 and SL3 (Figure 10). This implies that NAP tends to accumulate earlier in the dispersal process, reflecting short-distance transport, which is consistent with previous studies indicating NAP has concentrated in the nearshore areas of the Bohai Sea (Xu and Sun, 1988; Yang et al., 2019). In summary, in the proximal accumulations of the Huanghe prodelta, the percentage of SP and AP correlates positively with offshore dispersal, while that of NSP and NAP shows a negative correlation. Notably, this process is also influenced by the direction and strength of dispersal and the hydrodynamic regime, discussed further in Section 5.4.

The HST sediments in core H3 represent the Huanghe-dominated distal accumulation (Figure 1). Although its formation age is unclear, it provides an opportunity to compare pollen records between proximal and distal accumulations. The five proximal cores cover most of the evolutionary stages of the Huanghe delta, potentially including the timing for distal accumulation. Therefore, differences in pollen assemblages between core H3 and these cores can be attributed to disparities between proximal and distal accumulations. In core H3, the

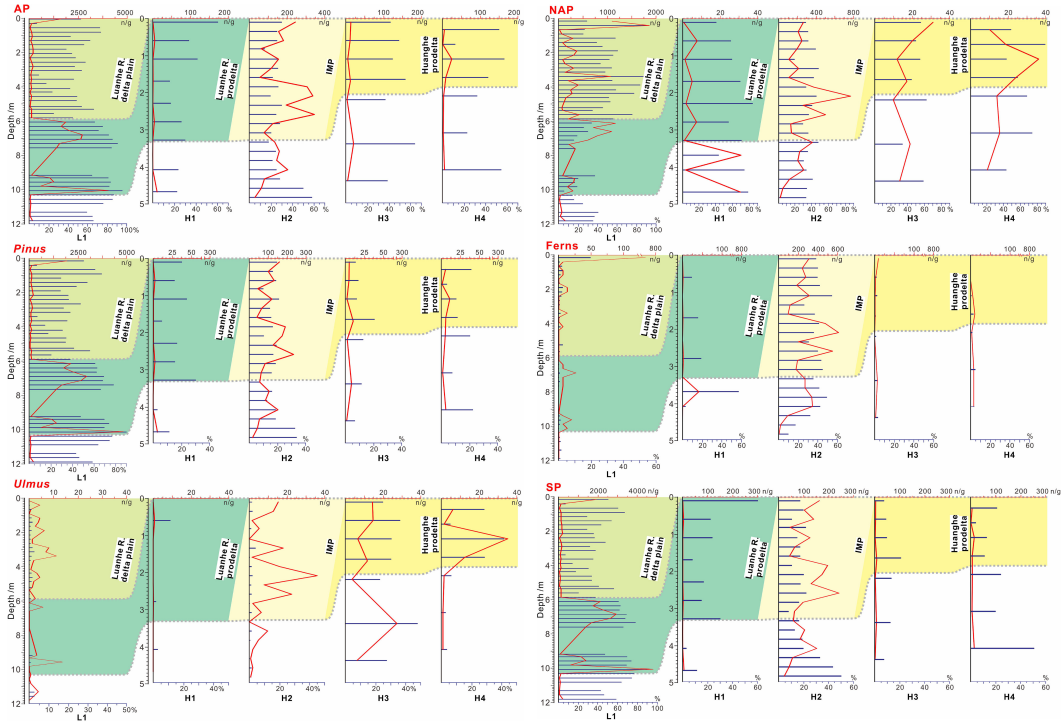

FIGURE 11
Concentration (grains/g; red curves) and percentage (navy bars) of representative pollen assemblages along the core transect in the northwestern Bohai Sea; See Figure 3 for the stratigraphic interpretation of the transect. Note that there is a mismatch in the proportions of cores L1 and cores H1-H4, and the Pleistocene sediments underlie the color-filled sections in each core. SP, saccate pollen; NSP, non-arboreal pollen.

percentage of AP is slightly lower than NAP, and *Pinus* percentage is insignificant (Figure 11). This indicates that, while AP, particularly *Pinus* pollen, can travel longer distances than NAP, both AP and NAP show low concentrations after extended long-distance transport, and the difference in their percentage observed in proximal sediments is no longer significant. Previous studies on seafloor sediments in the Bohai Sea suggest that wind-driven dispersal (in air) becomes the primary driver of pollen dispersal when water depth exceeds 20 m (Yang et al., 2019). However, this is not observed in core H3 (core top over 20 m water depth; Table 1), with lower SP and an insignificant percentage of *Pinus* (Figure 8). This could be due to complex pollen provenance and preservation processes in this distal mud, as further discussed in Section 5.3.

5.2 Pollen records in response to switching of delta lobes

Pollen records in deltaic-prodeltaic sediments were often used for paleoclimatic reconstruction (Hao et al., 2021; Ye et al., 2024). In the Huanghe delta, Yi et al. (2003) used variations in *Pinus* and NAP percentages in cores H9601 and H9602 to indicate climatic warmth and cooling. They associated a decrease in *Pinus* in Pollen Zone I/1 and Zone IIb/2 with a warm climate, while an increase in NAP and *Pinus* in Pollen Zone II/1 and Zone III/2 suggested cooling.

Our stratigraphic analysis (Figure 4) reveals that in core H9601, Zones I/1 and II/1 roughly correspond to SL2 and SL3, respectively, while in core H9602, Zone III/2 spans SL2, SL3, and superlobe V. In contrast to cores H9601 and H9602, where *Pinus* decreases in SL2 and increases in SL3, our core BHB1 shows the highest *Pinus* percentage in SL2 but a sharp decline in SL3, accompanied by an increase in NAP. Core YRD1 also does not exhibit an increase in NAP and *Pinus* in SL3; instead, both decrease slightly (Figure 10). This comparison highlights a noticeable variation in the vertical (downcore) distribution of pollen assemblages in prodeltaic sediments across different locations within the Huanghe delta. Given that significant changes occurred among different delta lobes, this variation is likely attributed to lobe switching, which involves alterations in offshore distance, sediment/pollen transport distance, and different time spans of accumulation (even for a single lobe, it may accumulate diachronously) across various sites.

In the northwestern Bohai Sea, core site L1 underwent a transition from a prodelta to a delta-plain environment due to recent lobe switching of the Luanhe River, which resulted in resulting in the shoreline protrusion and creation of deltaic land at this location (Yu, 2019; Liu et al., 2022) (Figures 1, 3). In prodeltaic sediments, the pollen assemblages are dominated by AP, particularly *Pinus* and *Quercus*, with AP significantly higher than NAP in percentages and concentrations (Figure 11, Supplementary Figure 4). In delta-plain

sediments, NAP becomes the dominant taxa, and the percentage of *Selaginella* is significantly higher than in prodeltaic sediments (Figure 11). Although the increased NAP and *Sela*ginella percentages in delta-plain sediments most likely associated with the transition in sedimentary facies related to lobe-switching, these changes might be alternatively interpreted as indicators of increased precipitation and more frequent river floods in pollen-based paleoclimatic studies. In earlier studies, these elements are typically used for as climatic indictors because *Selaginella* spores, being large in grains, settle and sediment primarily through river flooding (Xu et al., 1995), and NAP content is generally higher than AP during flooding periods (Xu et al., 2004). In addition, the decline in AP from prodeltaic to delta-plain sediments is also probably influenced more by lobe-switching-related changes in the sedimentary environment than by climate. Previous studies (e.g., Xu et al., 1995) have indicated a gradual decline in AP content with greater transport distance on the Luanhe River alluvial plain-delta plain. This pattern likely plays a significant role in the decline of AP during the prodelta to delta plain transition at core site L1, associated with increased onshore transport distance for this core site.

5.3 Impact of complex provenance on pollen records in distal accumulation

The northwestern Bohai Sea, receiving sediment from both the Huanghe and Luanhe River (Liu et al., 2022), is expected to show varied pollen assemblages in their prodeltas due to diverse vegetation in their drainage basins (Supplementary Figure S1B) (Yang et al., 2019). Along the core transect (Figure 3), HST sediments in core L1, representing Luanhe River input, displays a *Pinus-Artemisia-Quercus*-dominated pollen assemblage (Supplementary Figure S4), with the dominance of AP, which is consistent with offshore seafloor sediments (Xu and Sun, 1988). However, subsurface sediments within this offshore region, identified as the Huanghe-dominated mud belt distinct from the Luanhe River prodelta (Liu et al., 2022), exhibit variations from surface sediments and among themselves, showing *Artemisia-Ulmus*-Chenopodiaceae-*Pinus* (Figures 8, 9) with NAP dominance in cores H3 and H4 (Figure 11). Such a discrepancy in pollen assemblages between surface sediments and subsurface records, aligning otherwise with those of the separated Luanhe River delta, likely results from the abandonment of the Huanghe-dominated mud belt. We hypothesize that the mud belt has not received Huanghe supply for at least over 1 kyr; historical evidence indicates that the Huanghe flowed into the southern Yellow Sea between 1128 and 1855 CE (Liu et al., 2013), and there is no evidence of sediment supply from the Huanghe to the mud belt since 1855 CE (instead prone to disperse southeastward from MHD) when it re-entered the Bohai Sea (Liu et al., 2023). Thus, while subsurface pollen records may reflect the influence of the Huanghe, surface sediments appear to receive pollen sedimentation sourced from the surrounding region. This discovery underscores the complex nature of pollen provenance in seafloor sediments, especially during periods of sediment hiatus.

In cores H3 and H4, *Ulmus* dominates the AP, constituting ~41.2% of the total pollen assemblage (Figure 11). Notably, no such high content of *Ulmus* has been observed in sediment cores from the Luanhe River and Huanghe drainage basins, delta plains, or the Bohai Sea seafloor (Yi et al., 2003; Chen et al., 2012; Yang et al., 2019), where the representatives of AP are *Pinus*, *Quercus*, *Tilia*, and *Corylus* (Xu et al., 2007). Instead, *Ulmus* and other broad-leaved trees were dominant in the forests of the eastern Northeast China region during the early to mid-Holocene (Ren, 1999). Particularly, in the pollen assemblage of core DYD in the eastern Liaodong Peninsula, *Ulmus* pollen accounted for as much as 37.65% in Holocene sediments (Liu, 2022). As *Ulmus* is an airborne pollen primarily flowering from April to June, coinciding with prevailing southerly winds in the Bohai Sea area (Yang et al., 2019), we hypothesize that the *Ulmus* pollen in cores H3 and H4 originated from airborne and/or seawater dispersion from the Northeast China region rather than being transported with sediment from the Huanghe or Luanhe River. This hypothesis can be supported by the water depths of cores H3 and H4, both ~20 m (Table 1), and the Bohai Sea circulation system (Figure 1A); both facts favor westward transport from Northeast China, facilitating dispersion with water flow (cf., Yang et al., 2019). The abundant *Ulmus* pollen in cores H3 and H4 provides insights into how prodeltaic sediments preserve pollen from other regions through airborne and seawater dispersion during prodeltaic sedimentation, adding greater uncertainty and complexity to the pollen assemblages of prodeltaic sediments.

5.4 Pollen records in response to hydrodynamic regimes in terms of strength and direction

In the northwestern Bohai Sea, HST sediments in core H2 exhibit higher pollen concentrations (excluding *Ulmus*) than adjacent offshore cores H1, H3 and H4 (Figure 11 and Supplementary Figure 5), even surpassing delta-plain sediments in the onshore core L1 (Supplementary Figure 4), indicating that H2 is a pollen sink. Our stratigraphic analysis places core H2 in the erosion-dominated area with energetic longshore tidal currents (Xue et al., 2009), strong enough to remold the transgressive sand sheets into erosional sand ridges, but the core site is on an isolated mud patch filling a trough between the ridges, representing an area of accumulation/erosional relict (Liu et al., 2022) (Figures 2, 3). Despite the prevailing belief that quiescent conditions favor pollen deposition (Chmura and Eisma, 1995), the concentration of pollen in core H2 suggests that accumulations in energetic hydrodynamic conditions might provide an ideal setting for pollen deposition, potentially more so than in prodeltaic sediments (compared to cores H1, H3, and H4).

Fern spores, predominantly *Selaginella*, also exhibit the highest percentage and concentration in core H2 along the transect of the five cores (Figure 11), which can further support the afore mentioned

hypothesis. Specifically, *Selaginella* grains, as previously noted, being large and heavy, rely on strong hydrodynamic regimes for transport (Xu et al., 1995). Additionally, the high percentage of fern spores aligns with their buoyant nature, which allows them to be transported over longer distances (Dai and Weng, 2011; Dai et al., 2014; Yang et al., 2019). This nature may contribute to their high percentage in regions with strong transport regimes, particularly in seafloor sediments with increasing offshore distance and abundant precipitation, where fern spores far exceed pollen in percentage (Wang et al., 1987; Sun et al., 1999; van der Kaars and de Deckker, 2003).

Energetic longshore currents in the erosion-dominated area likely also influence pollen deposition in neighboring prodeltas, especially at their marginal parts. Cores H1 and H4, located at the boundary between the prodelta and the erosion-dominated area (Figures 1B; 3), represent such marginal sediments and exhibit lower pollen content compared to non-marginal core H3 (Figure 11). Additionally, we hypothesize that these currents control the sedimentation of *Ulmus* pollen along different zones. As *Ulmus* is likely transported from the east, possibly via seawater dispersal, strong longshore currents may act as a barrier, hindering *Ulmus* pollen from reaching more landward (northwestward) locations. This hypothesis explains the observed high *Ulmus* content in core sites (H3 and H4) southeast of the erosion-dominated area, while the content is much lower in the remaining cores (Figure 11).

Regionally, transport regimes can significantly impact pollen records, creating pollen sinks, due to their flow directions. This phenomenon is primarily observable in the western Bohai Sea, providing three lines of evidence. Firstly, an anomalous pattern in SL2 shows higher percentages of fern spores and *Quercus* near the river mouth in core H9601 but higher concentrations in core BHB1 farther away (Figure 10; Supplementary Figure 6). Despite typical nearshore concentration for *Quercus* (showing high percentages) in the western Bohai Sea (Yang et al., 2019) and an expected increase in fern percentage after long-distance transport, opposite trends for both elements were observed, potentially influenced by the local coastal current direction promoting nearshore pollen accumulation. Secondly, ferns exhibit nearshore concentration with percentages increasing offshore, a normal trend. However, the highest *Quercus* percentage and concentration appear in core H9602, not in core BHB1 closer to the contemporaneous river mouth (Figure 10; Supplementary Figure 1A), possibly due to core BHB1 being more offshore with deeper water depth, and the southeastward longshore transport regime at that time influencing a shallower region than core BHB1. The third evidence comes from total pollen concentration in core BHB1, which is the highest in both SL2 and SL3 (Figure 5). Given the core site BHB1 is neither the farthest nor closest to the contemporaneous river mouth for both SLs, the highest pollen concentration is most likely associated with a pollen sink likely induced by the local transport regime. Similar pollen sinks associated with the transport regime direction are observable in Bohai Sea surface sediments, particularly in Laizhou Bay (displaying the highest pollen concentration; Yang et al., 2019), a down-current region for the coastal current, indicating a sink (Figure 1A).

5.5 Impact of sediment grain size on pollen records

Considering that clinoform-scale construction of prodelta typically leads to specific arrangements of sediment grain size distribution (Patruno and Helland-Hansen, 2018), it is crucial to examine how this distribution affects the pollen records. We observed a positive correlation between grain size/mud content and pollen concentrations in various core segments (Figure 12). Specifically, in core BHB1, SL3 and SL2 exhibit the highest pollen concentrations (>4000 n/g; Figure 5) with the smallest grain size (clay or silt clay; Figure 4), while SL2 in core H9602 shows the lowest concentration (<50;Yi et al., 2003) with a significant increase in grain size (fine sand; Figure 4). In core L1, lower pollen concentrations are associated with coarser delta-plain sediments compared to the higher concentrations in prodeltaic sediments (Figures 3, 11).

This positive correlation, unsurprisingly, is also evident in seafloor sediments across various continental shelf regions, e.g., the northern South China Sea (Tong et al., 2012) and the Bohai Sea

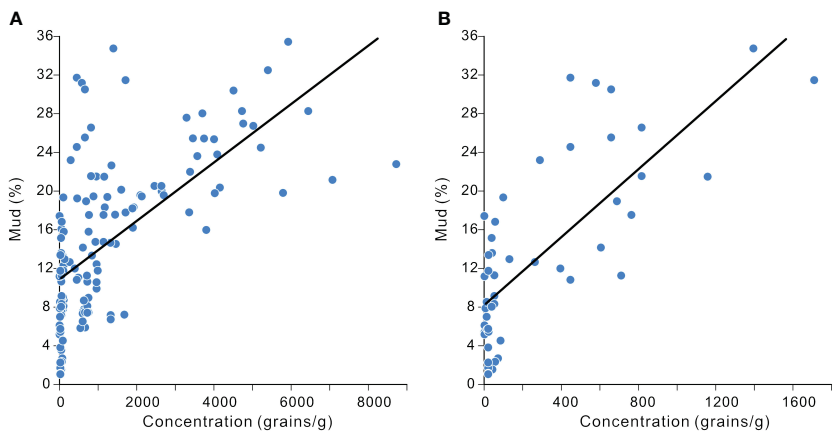

FIGURE 12
Correlation between total pollen concentration and mud percentage in sediment cores from the western Bohai Sea **(A)** and northwestern Bohai Sea **(B)**.

(Yang et al., 2019), likely attributed to the susceptibility of both pollen and fine-grained sediments to suspension-related dispersion in underwater conditions (Heusser, 1988). Nevertheless, in Huanghe prodelta sediments, this positive correlation is valid only when the mud content exceeds ~8-12%, and lower mud content may impede pollen accumulation (Figure 12).

6 Conclusions

In this study, we investigated the relationship between pollen and spore records and the stratigraphic evolution of the Huanghe-dominated prodelta, employing ten sediment cores (five new, five from literature) from both proximal and distal regions of the prodelta.

Our findings reveal that, in the proximal location of the Huanghe prodelta, variations in pollen assemblages, percentages, and concentrations among cores, as well as within different intervals within a single core, are dominated by avulsions and lobe switching of Huanghe, which were typically misattributed to climate change in earlier studies. Within a single delta lobe, pollen records are influenced by transport distance; typically, NAP and NSP percentages display an inverse relationship with distance, while AP and SP (particularly *Pinus*) percentages exhibit a positive correlation.

These patterns of pollen distribution in the proximal prodelta are absent in the distal accumulation of the prodelta (distal mud belt), suggesting a weakened connection with transport distance, following an extended period of transport. Instead, this Huanghe-dominated distal mud belt is characterized by a complex pollen provenance, sourced from both the surrounding regions and even more distant locations (e.g., the Liaodong Peninsula), rather than being dominated solely by Huanghe supply. The energetic longshore transport regime appears to favor deposition of pollens (especially *Quercus*) and fern spore in accumulation/erosional-relict areas within a condition of pervasive erosion. This regime also affects neighboring prodeltas, reducing pollen content at their marginal parts. Additionally, pollen concentration is controlled by sediment grain size distribution associated with prodelta evolution, with higher concentrations associated with more fine-grained sediments.

These findings underscore the constraints on pollen records in prodeltaic sediments, shaped by prodelta evolution, regional pollen provenance, and hydrodynamic conditions, which potentially surpass the impact of climate change. These complexities and uncertainties should be considered in pollen-based paleoenvironmental and paleoclimatic reconstructions in the delta/prodelta of Huanghe and other deltas worldwide. It is recommended to incorporate comprehensive stratigraphic, sedimentological and provenance analyses in conjunction with these studies.

Data availability statement

The raw data supporting the conclusions of this article will be made available by the authors, without undue reservation.

Author contributions

WH: Data curation, Formal analysis, Methodology, Visualization, Writing – original draft. SL: Conceptualization, Funding acquisition, Project administration, Supervision, Visualization, Writing – review & editing. YL: Data curation, Methodology, Supervision, Writing – review & editing. AF: Writing – review & editing. WF: Writing – review & editing. XW: Writing – review & editing. SC: Conceptualization, Funding acquisition, Project administration, Supervision, Writing – review & editing.

Funding

The author(s) declare financial support was received for the research, authorship, and/or publication of this article. This research received funding from the National Natural Science Foundation of China (grants 42076067, and 42276175).

Acknowledgments

This research received funding from the National Natural Science Foundation of China (grants 42076067, and 42276175). We extend our gratitude to the crews of the Research Center for Islands and Coastal Zone, First Institute of Oceanography, MNR, for their valuable contributions to data collection in the northwestern Bohai Sea. We appreciate three reviewers for their valuable inputs.

Conflict of interest

The authors declare that the research was conducted in the absence of any commercial or financial relationships that could be construed as a potential conflict of interest.

Publisher's note

Supplementary material

The Supplementary Material for this article can be found online at: https://www.frontiersin.org/articles/10.3389/fmars.2024.1378724/full#supplementary-material

References

Adojoh, O. C., Marret, F., Duller, R., Osterloff, P. L., Oboh-Ikuenobe, F. E., and Saylor, B. Z. (2023). Stages of palaeoenvironmental evolution, climate and sea level change of the Niger Delta, east Equatorial Atlantic: Novelty from elemental tracers, sedimentary facies and pollen records. *Holocene*. 33 (7), 781–790. doi: 10.1177/09596836231163506

Anthony, E. J., Gardel, A., Gratiot, N., Proisy, C., Allison, M. A., Dolique, F., et al. (2010). The Amazon-influenced muddy coast of South America: A review of mud-bank–shoreline interactions. *Earth-Science Rev.* 103, 99–121. doi: 10.1016/j.earscirev.2010.09.008

Beaudouin, C., Suc, J. P., Escarguel, G., Arnaud, M., and Charmasson, S. (2007). The significance of pollen signal in present-day marine terrigenous sediments: the example of the Gulf of Lions (western Mediterranean Sea). *Geobios* 40, 159–172. doi: 10.1016/j.geobios.2006.04.003

Chen, J. X., Shi, X. F., and Qiao, S. Q. (2012). Holocene palynological sequences and palaeoenvironmental changes in the Bohai Sea area. *Acta Oceanologica Sin.* 3, 99–105.

Cheng, G., and Xue, C. (1997). *Sedimentology of the Yellow River Delta* (Beijing: Geological Publishing House), 147.

Chmura, G. L., and Eisma, D. (1995). A palynological study of surface and suspended sediments on a tidal flat: implications for pollen transport and deposition in coastal waters. *Mar. Geology* 128, 183–200. doi: 10.1016/0025-3227(95)00096-H

Chmura, G. L., Smirnov, A., and Campbell, I. D. (1999). Pollen transport through distributaries and depositional patterns in coastal waters. *Palaeogeography Palaeoclimatology Palaeoecol.* 149, 257–270. doi: 10.1016/S0031-0182(98)00205-3

Correggiari, A., Cattaneo, A., and Trincardi, F. (2005). The modern Po Delta system: lobe switching and asymmetric prodelta growth. *Mar. Geology* 222, 49–74. doi: 10.1016/j.margeo.2005.06.039

Dai, L., and Weng, C. (2011). A survey on pollen dispersal in the western Pacific Ocean and its paleoclimatological significance as a proxy for variation of the Asian winter monsoon. *Sci. China Earth Sci.* 54, 249–258. doi: 10.1007/s11430-010-4027-7

Dai, L., Weng, C., Lu, J., and Mao, L. (2014). Pollen quantitative distribution in marine and fluvial surface sediments from the northern South China Sea: new insights into pollen transportation and deposition mechanisms. *Quaternary Int.* 325, 136–149. doi: 10.1016/j.quaint.2013.09.031

DeBusk, J. G.H. (1997). The distribution of pollen in the surface sediments of Lake Malawi, Africa, and the transport of pollen in large lakes. *Rev. Palaeobotany Palynology* 97, 123–153. doi: 10.1016/S0034-6667(96)00066-8

Di Rita, F., Celant, A., Milli, S., and Magri, D. (2015). Lateglacial–early Holocene vegetation history of the Tiber delta (Rome, Italy) under the influence of climate change and sea level rise. *Rev. Palaeobotany Palynology* 218, 204–216. doi: 10.1016/j.revpalbo.2014.12.005

Faegri, K., Kaland, P. E., and Krzywinski, K. (1989). *Textbook of pollen analysis. 4* (Chichester, UK: John Wiley & Sons Ltd).

Folk, R. L., and Ward, W. C. (1957). Branos river bar: a study in the significance of grain size parameter. *J. sedimentary Petrology* 27, 3–26. doi: 10.1306/74D70646-2B21-11D7-8648000102C1865D

Grimm, E. C. (1991). *TILIA v2.0.4 (Computer Software)* (Springfield, IL: Illinois State Museum, Research and Collections Centre).

Hait, A. K., and Behling, H. (2009). Holocene mangrove and coastal environmental changes in the western Ganga-Brahmaputra Delta, India. *Vegetation History Archaeobotany* 18, 159–169. doi: 10.1007/s00334-008-0203-5

Hao, X., Li, L., Ouyang, X., Culligan, N., Hu, B., Zhao, X., et al. (2021). Coastal morphodynamics and Holocene environmental changes in the Pearl River Delta, southern China: New evidence from palynological records. *Geomorphology* 389, 107846. doi: 10.1016/j.geomorph.2021.107846

He, L., Xue, C., Ye, S., Amorosi, A., Yuan, H., Yang, S., et al. (2019). New evidence on the spatial-temporal distribution of superlobes in the Yellow River Delta Complex. *Quaternary Sci. Rev.* 214, 117–138. doi: 10.1016/j.quascirev.2019.05.003

He, L., Xue, C., Ye, S., Laws, E. A., Yuan, H., Yang, S., et al. (2018). Holocene evolution of the Liaohe Delta, a tide-dominated delta formed by multiple rivers in Northeast China. *J. Asian Earth Sci.* 152, 52–68. doi: 10.1016/j.jseaes.2017.11.035

Heusser, L. E. (1988). Pollen distribution in marine sediments on the continental margin off northern California. *Mar. Geology* 80, 131–147. doi: 10.1016/0025-3227(88)90076-X

Heusser, L. E., and Balsam, W. L. (1985). Pollen sedimentation in the northwest Atlantic: effects of the Western Boundary Undercurrent. *Mar. Geology* 69, 149–153. doi: 10.1016/0025-3227(85)90138-0

Hooghiemstra, H., Lézine, A. M., Leroy, S. A., Dupont, L., and Marret, F. (2006). Late Quaternary palynology in marine sediments: a synthesis of the understanding of pollen distribution patterns in the NW African setting. *Quaternary Int.* 148, 29–44. doi: 10.1016/j.quaint.2005.11.005

IOCAS (Institute of Oceanography, Chinese Academy of Sciences) (1985). *Geology of the Bohai Sea* (Beijing: Science Press).

Korus, J. T., and Fielding, C. R. (2015). Asymmetry in Holocene river deltas: patterns, controls, and stratigraphic effects. *Earth-Science Rev.* 150, 219–242. doi: 10.1016/j.earscirev.2015.07.013

Leslie, A. B. (2010). Flotation preferentially selects saccate pollen during conifer pollination. *New Phytol.* 188, 273–279. doi: 10.1111/j.1469-8137.2010.03356.x

Li, X., Zhao, Y., Yang, Z., Qiao, S., Liu, B., Xie, Q., et al. (2023). Holocene marine deposits in the Bohai Sea: Depocenters, sediment sources, and oceanic and tectonic influences. *Geomorphology* 442, 108913. doi: 10.1016/j.geomorph.2023.108913

Li, Z., Saito, Y., Matsumoto, E., Wang, Y., Tanabe, S., and Vu, Q. L. (2006). Climate change and human impact on the Song Hong (Red River) Delta, Vietnam, during the Holocene. *Quaternary Int.* 144, 4–28. doi: 10.1016/j.quaint.2005.05.008

Liu, C. (2022). Analysis of sedimentary environment characteristics of boreholes in the eastern plain of the Dayang River area of eastern Liaoning. [M.S thesis]. Dalian, China: Liaoning Normal University.

Liu, S., Feng, A., Gao, S., Wang, Y. P., Jia, J., Du, J., et al. (2022). Evidence for a second deflected prodelta of the Yellow River: Insights into a complex pattern of delta asymmetry. *Mar. Petroleum Geology* 143, 105815. doi: 10.1016/j.marpetgeo.2022.105815

Liu, S., Feng, A., and Liu, Y. (2023). Buried channels under the northern Bohai Sea: Evidence for a great Bohai Paleolake during the late MIS3. *Mar. Pet. Geol.* 155, 106413. doi: 10.1016/j.marpetgeo.2023.106413

Liu, S., Feng, A., Liu, C., Zheng, Y., Li, P., and Zhang, Z. (2019). Seismic stratigraphy and morphology of the Holocene progradational system beneath Bohai Bay, Bohai Sea: Lobate evolution of a multi-sourced subaqueous fluviodeltaic complex. *Mar. Geology* 409, 31–47. doi: 10.1016/j.margeo.2018.12.009

Liu, S., Feng, A., Yang, L., Du, J., Yu, Y., Feng, W., et al. (2020). Stratigraphic and three-dimensional morphological evolution of the late Quaternary sequences in the western Bohai Sea, China: Controls related to eustasy, high sediment supplies and neotectonics. *Mar. Geology* 427, 106246. doi: 10.1016/j.margeo.2020.106246

Liu, J., Kong, X., Saito, Y., Liu, J. P., Yang, Z., and Wen, C. (2013). Subaqueous deltaic formation of the Old Yellow River (AD 1128–1855) on the western South Yellow Sea. *Mar. Geology* 344, 19–33. doi: 10.1016/j.margeo.2013.07.003

Liu, S., Li, P., Feng, A., Du, J., Gao, W., Xu, Y., et al. (2016b). Seismic and core investigation on the modern Yellow River Delta reveals the development of the uppermost fluvial deposits and the subsequent transgression system since the postglacial period. *J. Asian Earth Sci.* 128, 158–180. doi: 10.1016/j.jseaes.2016.07.009

Liu, J., Saito, Y., Wang, H., Zhou, L., and Yang, Z. (2009). Stratigraphic development during the Late Pleistocene and Holocene offshore of the Yellow River delta, Bohai Sea. *J. Asian Earth Sci.* 36, 318–331. doi: 10.1016/j.jseaes.2009.06.007

Liu, J., Wang, H., Wang, F., Qiu, J., Saito, Y., Lu, J., et al. (2016a). Sedimentary evolution during the last~ 1.9 Ma near the western margin of the modern Bohai Sea. *Palaeogeography Palaeoclimatology Palaeoecol.* 451, 84–96. doi: 10.1016/j.palaeo.2016.03.012

Lu, J., Huang, W., Sun, J., Wang, F., Gao, Y., Fan, X., et al. (2023). Quaternary pollen record and paleoenvironmental evolution of the Bohai Sea strait. *Regional Stud. Mar. Sci.* 68, 103278. doi: 10.1016/j.rsma.2023.103278

Luo, C., Chen, M., Xiang, R., Liu, J., Zhang, L., Lu, J., et al. (2013). Characteristics of modern pollen distribution in surface sediment samples for the northern South China Sea from three transects. *Quaternary Int.* 286, 148–158. doi: 10.1016/j.quaint.2012.11.001

Meng, G., and Wang, S. (1987). Studies on the quaternary sporo-pollen assemblage from the Bohai Sea drilling core BC-1 and its paleoclimate. *Oceanologia Limnologia Sin.* 18, 253–264.

Milliman, J. D., Yun-Shan, Q., Mei-e, R., and Saito, Y. (1987). Man's influence on the erosion and transport of sediment by Asian rivers: the Yellow River (Huanghe) example. *J. Geology* 95, 751–762. doi: 10.1086/629175

Mohapatra, P. P., Stephen, A., Prasad, S., Singh, P., and Anupama, K. (2019). Late Pleistocene and Holocene vegetation changes and anthropogenic impacts in the Cauvery delta plains, southern India. *Quaternary Int.* 507, 249–261. doi: 10.1016/j.quaint.2018.12.008

Mohapatra, P. P., Stephen, A., Singh, P., Prasad, S., and Anupama, K. (2021). Pollen based inference of Holocene sea level changes, depositional environment and climatic history of Cauvery delta, Southern India. *Catena* 199, 105029. doi: 10.1016/j.catena.2020.105029

Moore, P. D., Webb, J. A., and Collison, M. E. (1991). *Pollen analysis* (Oxford: Blackwell scientific publications).

Nakagawa, T., Kitagawa, H., Yasuda, Y., Tarasov, P. E., Nishida, K., Gotanda, K., et al. (2003). Asynchronous climate changes in the North Atlantic and Japan during the last termination. *Science* 299, 688–691. doi: 10.1126/science.1078235

Nilsson, S., Praglowski, J., and Nilsson, L. (1977). Atlas of airborne pollen grains and spores in northern Europe. *Verlag Natur och Kultur. Stockholm*. 160. doi: 10.1163/9789004612211

Ouyang, X., Hao, X., Culligan, N., Dai, L., Cheng, Z., and Li, S. (2021). Distribution of suspended sediments and pollen in the northern south China sea: Implications for pollen source, transport, and deposition in surface ocean waters. *Continental Shelf Res.* 231, 104600. doi: 10.1016/j.csr.2021.104600

Pantaléon-Cano, J., Yll, E. I., Pérez-Obiol, R., and Roure, J. M. (2003). Palynological evidence for vegetational history in semi-arid areas of the western Mediterranean (Almería, Spain). *Holocene* 13, 109–119. doi: 10.1191/0959683603hl598rp

Patruno, S., and Helland-Hansen, W. (2018). Clinoforms and clinoform systems: Review and dynamic classification scheme for shorelines, subaqueous deltas, shelf edges and continental margins. *Earth-Science Rev.* 185, 202–233. doi: 10.1016/j.earscirev.2018.05.016

Qin, Y., Zhao, Y., Chen, L., and Zhao, S. (1990). Geology of Bohai Sea. *China Ocean Press Beijing* pp, 1–354.

Rahman, A., Luo, C., Chen, B., Haberle, S., Khan, M. H. R., Jiang, W., et al. (2020). Regional and seasonal variation of airborne pollen and spores among the cities of South China. *Acta Ecologica Sin.* 40, 283–295. doi: 10.1016/j.chnaes.2019.05.012

Reimer, P. J., Austin, W. E., Bard, E., Bayliss, A., Blackwell, P. G., Ramsey, C. B., et al. (2020). The IntCal20 Northern Hemisphere radiocarbon age calibration curve (0–55 cal kBP). *Radiocarbon* 62, 725–757. doi: 10.1017/RDC.2020.41

Ren, G. Y. (1999). Pollen distribution map and analysis of Holocene in northeast China. *Acta Palaeontologica Sin.* 38, 365–385.

Saito, Y., Wei, H., Zhou, Y., Nishimura, A., Sato, Y., and Yokota, S. (2000). Delta progradation and chenier formation in the Huanghe (Yellow River) delta, China. *J. Asian Earth Sci.* 18, 489–497. doi: 10.1016/S1367-9120(99)00080-2

Schwendemann, A. B., Wang, G., Mertz, M. L., McWilliams, R. T., Thatcher, S. L., and Osborn, J. M. (2007). Aerodynamics of saccate pollen and its implications for wind pollination. *Am. J. Bot.* 94, 1371–1381. doi: 10.3732/ajb.94.8.1371

Shepard, F. P. (1954). Nomenclature based on sand-silt-clay ratios. *J. Sedimentary Res.* 24, 151–158. doi: 10.1306/D4269774-2B26-11D7-8648000102C1865D

Smith, V., Warny, S., Jarzen, D. M., Demchuk, T., Vajda, V., and Gulick, S. P. (2020). Paleocene-Eocene palynomorphs from the Chicxulub impact crater, Mexico. Part 2: angiosperm pollen. *Palynology* 44, 489–519. doi: 10.1080/01916122.2019.1705417

Song, B., Li, Z., Lu, H., Mao, L., Saito, Y., Yi, S., et al. (2017). Pollen record of the centennial climate changes during 9-7 cal ka BP in the Changjiang (Yangtze) River Delta plain, China. *Quaternary Res.* 87, 275–287. doi: 10.1017/qua.2017.1

Stuiver, M., Reimer, P. J., and Reimer, R. W. (2022) *Calib 8.2.* Available online at: http://calib.org.

Su, J., and Yuan, Y. (2005). *China Offshore Hydrology* (Beijing: Ocean Press).

Sun, X., Li, X., and Beug, H. J. (1999). Pollen distribution in hemipelagic surface sediments of the South China Sea and its relation to modern vegetation distribution. *Mar. Geology* 156, 211–226. doi: 10.1016/S0025-3227(98)00180-7

Tang, L., Mao, L., Shu, J., Li, C., Shen, C., and Zhou, Z. (2020). *Atlas of Quaternary pollen and spores in China* (Singapore: Springer Nature). doi: 10.1007/978-981-13-7103-5

Tian, L. (2010). *Deglacial Sequence and Sedimentary Evolution in the West Bohai Bay, China* (Beijing: Phd Thesis of China University of Geosciences (Beijing).

Tian, L., Chen, Y., Jiang, X., Wang, F., Pei, Y., Chen, Y., et al. (2017). Post-glacial sequence and sedimentation in the western Bohai Sea, China, and its linkage to global sea-level changes. *Mar. Geology* 388, 12–24. doi: 10.1016/j.margeo.2017.04.006

Tian, F., Xu, Q., Li, Y., Cao, X., Wang, X., and Zhang, L. (2008). Pollen assemblage characteristics of lakes in the monsoon fringe area of China. *Chin. Sci. Bull.* 53, 3354–3363. doi: 10.1007/s11434-008-0408-0

Tong, G., Chen, L., Long, J., Li, T., Xiao, X., and Tong, S. (2012). Surface pollen distribution patterns in Beibu Gulf and corresponding sediment dynamics environment. *Chin. Sci. Bull.* 57, 902–911. doi: 10.1007/s11434-011-4912-2

van der Kaars, S. (2001). Pollen distribution in marine sediments from the south-eastern Indonesian waters. *Palaeogeography Palaeoclimatology Palaeoecol.* 171, 341–361. doi: 10.1016/S0031-0182(01)00253-X

van der Kaars, S., and de Deckker, P. (2003). Pollen distribution in marine surface sediments offshore Western Australia. *Rev. Palaeobotany Palynology* 124, 113–129. doi: 10.1016/S0034-6667(02)00250-6

Wang, K. (1993). *Spore-pollen and algal assemblages in the sediments of the Bohai Sea and palaeoenvironments* (Beijing: Geological Publishing House).

Wang, H. (2013). *Climate Change around Bohai Region during 1956 to 2011 and its Relationship with ENSO. M.D* (Thesis of Northwest Normal University).

Wang, F., Qian, N., Zhang, Y., and Yang, H. (1995). *Pollen Flora of China* (Beijing: Science Press), 1–461.

Wang, K., Sun, Y., Zhang, Y., Jiang, H., and Zhang, Y. (1987). *The Spore-Pollen and Algal Assemblage in the East China Sea Sediments* (Beijing: China Ocean Press), 10–80.

Wang, H., Yang, Z., Saito, Y., Liu, J. P., Sun, X., and Wang, Y. (2007). Stepwise decreases of the Huanghe (Yellow River) sediment load (1950–2005): Impacts of climate change and human activities. *Global Planetary Change* 57, 331–354. doi: 10.1016/j.gloplacha.2007.01.003

Wodehouse, R. P. (1935). *Pollen grains. Their structure, identification and significance in science and medicine* (London: Mc Graw-Hill Publishing Co. Ltd.).

Xiong, X. (2012). *Chinese Offshore Oceanography – Physical Oceanography and Marine Meteorology* (Beijing: Ocean Press).

Xu, Q., Li, Y., Yang, X., and Zheng, Z. (2007). Quantitative relationship between pollen and vegetation in northern China. *Sci. China Ser. D: Earth Sci.* 50, 582–599. doi: 10.1007/s11430-007-2044-y

Xu, Q., Yang, X., Wu, C., Meng, L., and Wang, Z. (1996). Alluvial pollen on the North China plain. *Quat. Res.* 46 (3), 270–280. doi: 10.1006/qres.1996.0066

Xu, J., and Sun, T. (1988). The assemblage feature of the spore-pollen in the surface sediments of the western Bohai Sea. *Bull. Mar. Sci.* 7, 49–54.

Xu, Q., Yang, X. L., Wang, Z., Wu, C., Meng, L., and Yao, Z. (1995). Study on pollen transportation by rivers. *Acta Botanica Boreali-Occidentalia Sin.* 37, 829–832.

Xu, Q., Yang, X., and Yang, Z. (2004). Relationship between pollen assemblages and vegetation in alluvial sediments of Luanhe River Basin. *J. Palaeogeogr.* 6, 69–77s.

Xu, Q., Zhang, S., Gaillard, M. J., Li, M., Cao, X., Tian, F., et al. (2016). Studies of modern pollen assemblages for pollen dispersal-deposition-preservation process understanding and for pollen-based reconstructions of past vegetation, climate, and human impact: a review based on case studies in China. *Quaternary Sci. Rev.* 149, 151–166. doi: 10.1016/j.quascirev.2016.07.017

Xue, C. (1993). Historical changes in the Yellow River delta, China. *Mar. geology* 113, 321–330. doi: 10.1016/0025-3227(93)90025-Q

Xue, C. T. (2009). Historical changes of coastlines on west and south coasts of Bohai Sea since 7000 a BP. *Scientia Geographica Sin.* 29, 217–222. doi: 10.13249/j.cnki.sgs.2009.02.217

Xue, C., and Cheng, G. (1989). "Shelly ridges in west coast of Bohai Sea and Holocene Yellow River delta system," in *Quaternary Processes and Events in China Offshore and Onshore Areas*. Eds. Z. Yang and H. Lin (China Ocean Press, Beijing), 117–125.

Xue, Z., Feng, A., Yin, P., and Xia, D. (2009). Coastal erosion induced by human activities: A northwest Bohai Sea case study. *J. Coast. Res.* 25, 723–733. doi: 10.2112/07-0959.1

Xue, C., Qin, Y., Ye, S., Laws, E. A., and Wang, Z. (2018). Evolution of Holocene ebb-tidal clinoform off the Shandong Peninsula on East China Sea shelf. *Earth-Science Rev.* 177, 478–496. doi: 10.1016/j.earscirev.2017.12.012

Yang, Z., and Liu, J. P. (2007). A unique Yellow River-derived distal subaqueous delta in the Yellow Sea. *Mar. Geology* 240, 169–176. doi: 10.1016/j.margeo.2007.02.008

Yang, S., Song, B., Ye, S., Laws, E. A., He, L., Li, J., et al. (2019). Large-scale pollen distribution in marine surface sediments from the Bohai Sea, China: Insights into pollen provenance, transport, deposition, and coastal-shelf paleoenvironment. *Prog. Oceanography* 178, 102183. doi: 10.1016/j.pocean.2019.102183

Yao, Q., Liu, K. B., Aragón-Moreno, A. A., Rodrigues, E., Xu, Y. J., and Lam, N. S. (2020). A 5200-year paleoecological and geochemical record of coastal environmental changes and shoreline fluctuations in southwestern Louisiana: implications for coastal sustainability. *Geomorphology* 365, 107284. doi: 10.1016/j.geomorph.2020.107284

Yao, Q., Rodrigues, E., Liu, K. B., Snyder, C., and Culligan, N. (2022). A Late-Holocene palynological record of coastal ecological change and climate variability from Apalachicola, Florida, USA. *Climate Change Ecol.* 3, 100056. doi: 10.1016/j.ecochg.2022.100056

Ye, L., Gao, L., Han, M., Li, Y., Xiao, X., and Long, H. (2024). The late Quaternary palynological record of the northern Yangtze Delta: Implication for palaeoclimate change in East Asia. *Catena* 234, 107630. doi: 10.1016/j.catena.2023.107630

Yi, S., Saito, Y., Oshima, H., Zhou, Y., and Wei, H. (2003). Holocene environmental history inferred from pollen assemblages in the Huanghe (Yellow River) delta, China: climatic change and human impact. *Quaternary Sci. Rev.* 22, 609–628. doi: 10.1016/S0277-3791(02)00086-0

Yi, S., Saito, Y., and Yang, D. (2006). Palynological evidence for Holocene environmental change in the Changjiang (Yangtze River) delta, China. *Palaeogeography Palaeoclimatology Palaeoecol.* 241, 103–117. doi: 10.1016/j.palaeo.2006.06.016

Yu, X. (2019). Sedimentary characteristics and evolutions of the Luan River Delta during the Holocene. [Phd thesis]. (Beijing: Institute of Oceanlogy, Chinese Academy of Sciences).

Zang, Q. (1996). *Nearshore Sediment along the Yellow River Delta* (Beijing: Ocean Press).

Zhao, X., Thomas, I., Salem, A., Alassal, S. E., Liu, Y., Sun, Q., et al. (2020). Holocene climate change and its influence on early agriculture in the Nile Delta, Egypt. *Palaeogeography Palaeoclimatology Palaeoecol.* 547, 109702. doi: 10.1016/j.palaeo.2020.109702